Geophysical Journal International

Geophys. J. Int. (2023) **232,** 1006–1030
Advance Access publication 2022 August 26
GJI Gravity, Geodesy and Tides

https://doi.org/10.1093/gji/ggac340

Data-driven multi-step self-de-aliasing approach for GRACE and GRACE-FO data processing

Petro Abrykosov,[1] Michael Murböck,[2] Markus Hauk,[3,4,5] Roland Pail[1] and Frank Flechtner[2,3]

[1]*Chair of Astronomical and Physical Geodesy, Technical University of Munich (TUM), Arcisstraße* 21, 80333 *München, Germany.*
E-mail: petro.abrykosov@tum.de
[2]*Physical Geodesy, Technische Universität Berlin, Straße des* 17. *Juni* 135, 10623 *Berlin, Germany*
[3]*Helmholtz Centre Potsdam, GFZ German Research Centre for Geosciences, Section* 1.2*: Global Geomonitoring and Gravity Field, Telegrafenberg,* 14473 *Potsdam, Germany*
[4]*Max-Planck-Institute for Gravitational Physics (Albert-Einstein-Institute), Leibnitz University Hannover, Callinstraße* 38, 30167 *Hannover, Germany*
[5]*German Aerospace Center (DLR), Institute for Satellite Geodesy and Inertial Sensing, Callinstraße* 30*b,* 30167 *Hannover, Germany*

Accepted 2022 August 24. Received 2022 August 23; in original form 2022 June 4

SUMMARY

Temporal aliasing errors resulting from the undersampling of non-tidal atmospheric as well as oceanic mass variations constitute the largest limitation towards the retrieval of monthly gravity solutions based on GRACE and GRACE-FO satellite gravity missions. Their mitigation is thus a primary goal of current research. Unfortunately, the two-step co-parametrization approach proposed for application in Bender-type gravity retrieval scenario in Wiese *et al.* yields no added value for a single satellite pair. A detailed study of this parametrization strategy is carried out and it is shown that the reason for this is the flawed central assumption of the proposed method, that is that signals of different spatial wavelengths can be perfectly captured and separated with respect to their temporal extent. Based on this finding, we derive a multi-step self-de-aliasing approach (DMD) which aims to rectify the shortcoming of the Wiese *et al.* method specifically for the single-pair case while retaining its independence from background-model-based de-aliasing of non-tidal atmosphere and ocean (AO) signal components. The functionality and added value of this novel approach is validated within a set of numerical closed-loop simulations as well as in real GRACE and GRACE-FO data processing. The simulation results show that the DMD may improve the gravity retrieval performance in the high-degree spectrum by more than one order of magnitude if one aims to retrieve the full AOHIS (i.e. atmosphere, ocean, hydrology, ice, solid earth) signal, and by at least a factor 5 if *a priori* AO de-aliasing is applied. Simultaneously, the DMD is shown to degrade the retrieval of the low degrees, but it is also demonstrated that this issue can be mitigated by introducing a constraint into the processing scheme. The simulation results are widely confirmed by results obtained from applying the DMD to real GRACE/GRACE-FO data of the test years 2007, 2014 and 2019. The applicability of the DMD is further shown for Bender-type gravity retrieval. It is demonstrated that in case of a double-pair-based gravity retrieval this approach is at least equivalent to the Wiese *et al.* method.

Key words: Satellite gravity; Time variable gravity.

1 INTRODUCTION

Satellite-based gravimetry is the only observation technique which allows for a direct quantification of mass redistributions within the Earth System on a global scale and with homogenous accuracy. Especially the Gravity Recovery And Climate Experiment twin-satellite mission (GRACE; Tapley *et al.* 2004; Flechtner *et al.* 2021), operational from 2002 to 2017, has provided the scientific community with revolutionary insights into a wide range of geodynamic processes primarily related to continental hydrology (e.g. Reager *et al.* 2014; Abelen *et al.* 2015; Mulder *et al.* 2015) and ice mass balance (e.g. Shepherd *et al.* 2012; Velicogna *et al.* 2014). Since 2018 the observation time series is being continued by the successor mission GRACE Follow-On (GRACE-FO; Kornfeld *et al.* 2019).

Extracting the target information related to processes within hydrology, ice and solid Earth (HIS) from GRACE/GRACE-FO observations is not a trivial task, as it is to a wide extent superimposed by a multitude of disturbing signals. The main error contributors here are the ocean tides (OT) and non-tidal variations within the atmosphere and ocean (AO). Their short-periodic components cannot be adequately resolved due to the limited temporal resolution of single satellite pair observations, and thus result in temporal aliasing effects within the retrieved gravity solutions. Therefore, *a priori* de-aliasing based on geophysical background models (BM) is employed in GRACE/GRACE-FO data processing in order to mitigate this issue (Dobslaw *et al.* 2013). The Atmosphere and Ocean De-Aliasing Product (AOD1B) is routinely computed by the GRACE Science Data System to provide a time-variable background model for the removal of non-tidal high-frequency mass signals from the sensor data (AOD1B RL06; Dobslaw *et al.* 2017). A new release AOD1B RL07, which is based on operational ECMWF and ERA-5 Reanalysis Data, is currently in preparation (Shihora *et al.* 2022). The 1-hourly AOD product HUST-ERA5 (Yang *et al.* 2021) is based on ERA5 climate data and shows an overall agreement with AOD1B-RL06 with a correlation of 0.99, but also considerable regional discrepancies. The impact of AOD1B products on precise orbits of altimetry satellites and altimetry results is investigated by Rudenko *et al.* (2016), demonstrating that the use of AOD1B products reduces the scatter of radial errors by up to 3 per cent, and an improved consistency among various altimeter mission of up to 10 per cent. However, since any applied BM inevitably features some level of imperfection, residual aliasing effects still notably affect the retrieved gravity fields in the form of the typical north–south striping pattern (Flechtner *et al.* 2016).

Next to the obvious requirement of improving the BMs' quality in order to reduce temporal aliasing, the application of more eloquent processing strategies can also be considered. With regard to the reduction of OT-induced aliasing, the direct co-estimation of OT constituents whose excitation frequencies are well-known was already successfully applied to real GRACE data (Han *et al.* 2007; Killet *et al.* 2011; Mayer-Gürr *et al.* 2012). In Hauk & Pail (2018) an improved feasibility of this approach was shown for gravity retrieval based on Bender-type double-pair missions. A different approach proposed in Abrykosov *et al.* (2021) has demonstrated the reduction of OT-related aliasing effects in numerical closed-loop simulation studies by stochastically modelling the spatial error distribution of OT models and propagating this error information onto the level of observations.

On the side of AO, the performance of de-aliasing can also be increased by incorporating model error information into the gravity adjustment process, as was shown in Kvas & Mayer-Gürr (2019). A direct co-estimation of signal-components similar to OT is not realistically feasible in this case, because the AO signal is composed of a vast multitude of individual components whose exact spatial extent, amplitudes and underlying excitation frequencies for the most part cannot be predicted or are not known at all. Nevertheless, it is known that the strongest AO signals occur on large spatial scales over short time periods of maximum a few days (shown e.g. in Daras & Pail 2017; Fig. 1). Based on this knowledge, a parametrization scheme for double-pair-based gravity processing has been introduced in Wiese *et al.* (2011) (in the following denoted as 'two-step co-parametrization') where in addition to the high degrees of a monthly gravity solution low-resolution fields are co-estimated over short time intervals. This method aims to explicitly parametrize the long-wavelength, high-amplitude AO signals into the interval fields, thus preventing them from leaking into the high-degree spectrum and facilitating an enhanced retrieval of the full AOHIS (i.e. atmosphere, ocean, hydrology, ice, solid earth) signal. Although the functionality of the two-step co-parametrization approach has been demonstrated in multiple science studies for Bender-type double-pair mission constellations (e.g. Daras 2016; Daras & Pail 2017; Purkhauser *et al.* 2020), no added value could be asserted for GRACE-type processing. Now, detailed system studies in the framework of the Research Unit NEROGRAV funded by the German Research Foundation have revealed a major flaw in the underlying assumptions of the two-step co-parametrization approach. Following these newly gained insights, we present a novel self-de-aliasing approach for single-pair-based gravity retrieval which is independent of prior knowledge on the AO component and in this regard therefore data-driven. In addition to the enhanced retrieval performance of the monthly gravity product, this self-de-aliasing approach also yields reliable stand-alone gravity solutions for short-time intervals which may be of potential value for near-real-time (NRT) applications.

The manuscript is structured as follows. In Section 2, a brief review of the standard two-step co-parametrization scheme from Wiese *et al.* (2011) is given, and its shortcomings are pointed out and discussed. Based on these findings we present the previously denoted novel data-driven self-de-aliasing approach for an enhanced AOHIS retrieval in the frame of a single-pair mission scenario in Section 3. A detailed discussion on the functionality and potential drawbacks of this method is also given. In Section 4, the added value of this novel de-aliasing strategy is then validated and quantified in a series of numerical closed-loop simulations, and an outlook towards its applicability to double-pair-based gravity retrieval is given. In Section 5, the novel parametrization scheme is validated in real GRACE and GRACE-FO data processing. Finally, the key results are summarized in Section 6, and an outlook is given towards potential future refinements and remaining open questions.

2 REVIEW OF 'TWO-STEP CO-PARAMETRIZATION' PROPOSED BY Wiese *et al.* (2011)

The value of the self-de-aliasing approach developed in Wiese *et al.* (2011) has been shown in the scope of Bender-type mission constellations, that is a GRACE-like polar satellite pair complemented by an additional satellite pair flying at a lower inclination (Bender *et al.* 2008), in numerous science studies related to Next Generation Gravity Field Missions (NGGM; Daras 2016; Daras & Pail 2017; Purkhauser *et al.* 2020). In this approach, low-resolution fields [e.g. up to degree and order (d/o) 15] are co-estimated over subsequent short (e.g. daily) time intervals alongside the higher-degree spherical harmonic coefficients (in this example from d/o 16 upwards) which is estimated over a longer (typically monthly) period. In Purkhauser & Pail (2019) it was demonstrated that this parametrization scheme yields accurate short-term gravity estimates, which may be of great interest of potential NRT-type applications. However, its primary value is the ability to capture

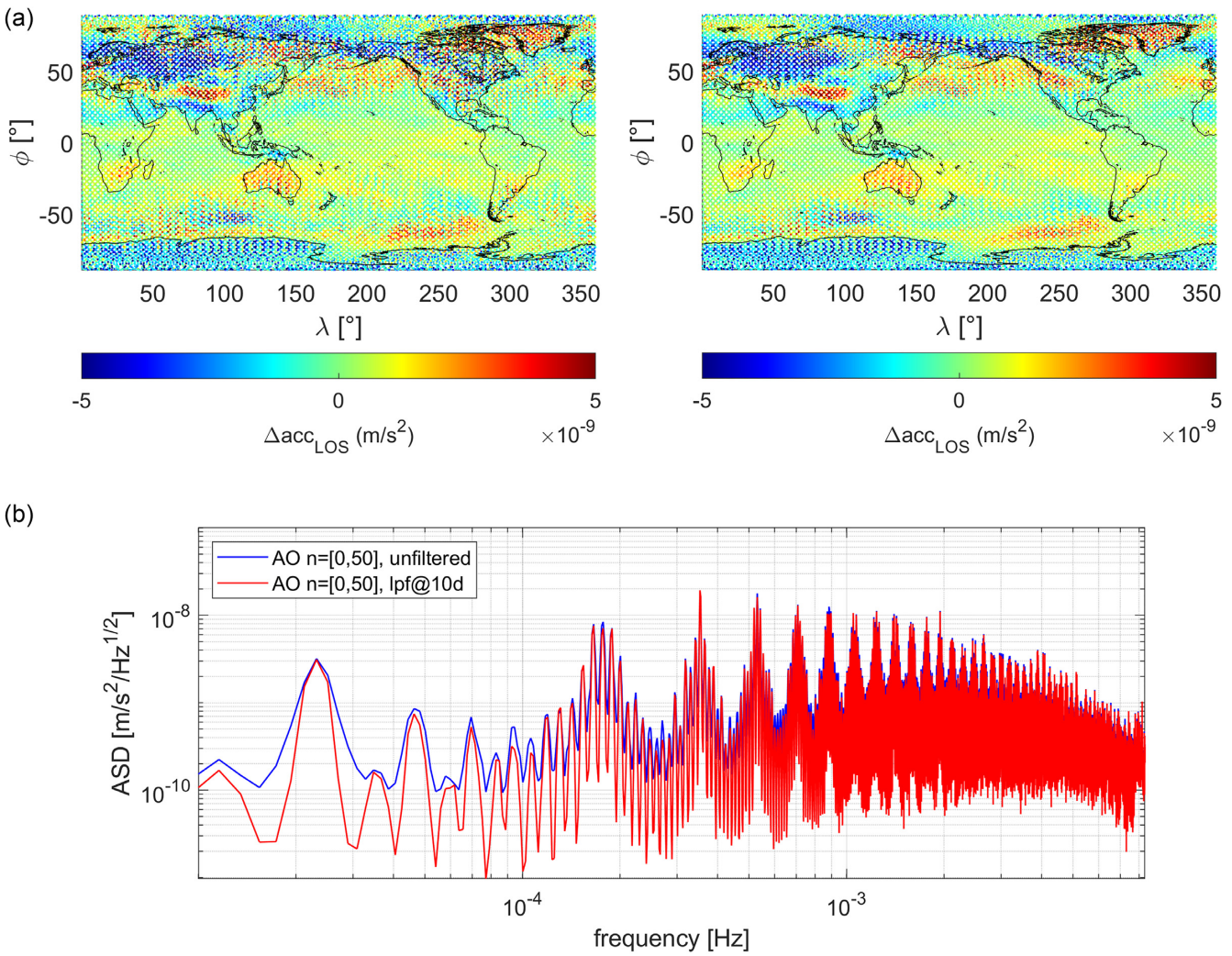

Figure 1. Range accelerations time series as observed by the polar satellite pair in a simulation environment. (a) shows the observations along the ground track which have been obtained based on the true AO signal (left) and a 10-d low-pass-filtered AO signal (right; i.e. all signal components with periods shorter than 10 d have been removed for any given point in space). (b) shows the amplitude spectral densities of these two observation time series.

short-periodic high-amplitude signal components, by their nature mostly related to AO and OT, in the interval solutions. As a consequence, the temporal aliasing of these short-term signals into the high degrees of the long-term estimate can be reduced significantly, thus improving the performance of the latter. In this regard, all aforementioned science studies have made the central assumption that all signal constituents with periods longer than twice the interval length of the co-estimated short-term solutions, for example 2 d in the case of daily co-estimates, can be perfectly mapped according to the Nyquist–Shannon sampling theorem (Shannon 1949).

However, it can be shown with a simple experiment that this assumption is flawed. We assume a GRACE-type polar satellite pair, for which we accumulate observations over a period of 30 d in a simulation environment (*cf.* Section 4) for two scenarios. In the first scenario, the observations are based exclusively on the Updated ESA Earth System Model's (Dobslaw *et al.* 2014) AO components provided in terms of Stokes' coefficients at 6-hourly intervals while in the second scenario, a low-pass filter with a cut-off frequency of 10 d is applied first to the 30-d time series of each underlying AO Stokes' coefficient. In this way, all input signal components with periods of less than 10 d are removed for any given geolocation.

The resulting observation time series along the satellite pair's orbit are compared in both the spatial and the spectral domain in Fig. 1. It is notable that while any given geolocation now indeed does not feature any signal components of less than 10 d, the satellite pair's observation time series remains almost unchanged. The reason for this is the satellite pair's near-complete insensitivity to geolocation-specific signal evolutions conditioned by the underlying spatio-temporal sampling. In other words, while a multitude of signals of various spatial extents occur simultaneously over the entire globe, the satellite pair only captures snapshots of these along its ground track at specific epochs while ignoring everything else, which in turn results in a heavily aliased observation time series. It is clear that such a high-frequency spatial signal distribution cannot be parametrized adequately by a low-degree parameter model (e.g. up to degree/order 15 at daily intervals). An accurate separation with regard to the underlying AO signal's spatial and temporal content would only be feasible if each component was to be observed

simultaneously and continuously throughout its occurrence. This is, of course, a purely hypothetic statement since the availability of a vast number of satellite pairs would be required to realize such a homogenous coverage with respect to space and time.

While a perfect separation of signal components through the two-step co-parametrization approach can neither be achieved in case of a single- nor in case of a double-pair-based retrieval, an increase in retrieval performance can already be expected even if only part of the signals is parametrized correctly. Fig. 2(a) indicates that such a partial signal separation is indeed possible. Here, the two-step co-parametrization was applied to 30 d of AOHIS-only-based observations of a single- and a double-pair scenario and the interval fields (daily up to d/o 7 and d/o 15, respectively) could be estimated with sufficient accuracy in both cases. However, while the corresponding double-pair-based monthly field obtained with the two-step scheme features some significant improvements in comparison to the solution retrieved with the nominal processing (i.e. no additional (co-)parametrization applied) in certain spectral bands, the single-pair-based equivalents feature the exact opposite behaviour. Fig. 2(b) shows the correlation matrices of the estimated Stokes' coefficients for the aforementioned scenarios, which—as the inverses of the respective normal equation systems (NEQ) without the inclusion of stochastic modelling—depend exclusively on the observation geometry and the chosen parametrization. It is evident that the co-estimation of short-term gravity parameters induces notable correlations of up to 60 per cent between nearly all coefficient groups in the single-pair case, whereas in a double-pair scenario they are significantly reduced in amplitude to overall less than 10 per cent except for some rare exceptions. Consequently, any erroneous parametrization of any signal will inevitably affect all short- as well as the long-term solutions, which in turn leads to an overall degradation of the monthly retrieval. On the contrary, due to the reduced correlations between coefficient groups in the double-pair case, the corresponding misparametrization error is smaller in comparison to the improvements attributed to the correct decoupling of signals.

In other words, the Bender-type observation geometry implicitly introduces an important constraint to the two-step co-parametrization approach. This is further demonstrated in Fig. 2(c). Here, it is evident that due to the short-periodic nature of the long-wavelength AO signals in combination with the near-polar orbit geometry the observations feature a distinct north–south striping pattern in the spatial domain in case of a single-pair scenario. Applying the nominal retrieval scheme would therefore result in large-scale errors in the high-degree spectrum, that is temporal aliasing. Taking into account the drawbacks presented earlier, the two-step co-parametrization cannot be expected to notably improve this issue, as the only constraint towards the parametrization of short-periodic signal components in this case is the time, that is the intervals at which the interval fields are set up. If an additional satellite pair is included, however, the stripes within the observations turn into a far more isotropic pattern in the latitudes between $\pm$ 70°. The short-periodic signal components are still fully present in the observations, but the favourable observation geometry effectively prevents the two-step scheme from mapping short-periodic long-wavelength signals into the high-degree spectrum.

In summary, it is evident that the single-pair-based estimation of long-term gravity solutions cannot benefit from the two-step co-parametrization approach in its nominal form, firstly due to the violation of its central hypothesis, and secondly due to the reduced numeric stability of the underlying NEQ system. However, taking into account the fact that the interval fields can nevertheless be retrieved with a sufficiently high accuracy, it is reasonable to assume that estimating the low-degree interval solutions independently of the high degrees of the monthly field can at least reduce the impact of the second effect.

3 DATA-DRIVEN MULTI-STEP SELF-DE-ALIASING APPROACH (DMD)

Based on the findings in chapter 2, we present a data-driven (in the sense that no background-model-based *a priori* AO de-aliasing is applied) multi-step self-de-aliasing approach (abbreviated as DMD) which aims to improve the performance of primarily single-pair-based gravity retrieval. Here, the observations which are based on—amongst others—the full AOHIS signal are split into intervals of e.g. one day of length for which individual low-resolution gravity fields up to a certain spherical harmonic degree n_{int} are estimated, disregarding the fact that the observations contain also high-degree signals and thus allowing for a certain amount of spectral leakage. These fields then represent valid stand-alone gravity solutions for the respective interval and are further used to compute reference observations which in a subsequent step are reduced from the original ones. Based on the reduced observations we then estimate a long-term, for example monthly, solution from d/o 0 up to a certain $n_{\max}$ (where $n_{\max} > n_{\text{int}}$) and, in a final step, restore the (weighted) mean of the interval estimates to the low degrees of the long-term solution. The explicit separation between the estimation of interval solutions and the long-term one follows the necessity of decorrelating both components at least in the case of a single-pair-based retrieval, which has been demonstrated in the previous section.

It is emphasized that the DMD's underlying principle is not comparable to that of the regular background-model-based de-aliasing, as the DMD does not explicitly remove the disturbing AO components. Instead, similarly to the originally envisioned principle of the method shown in Wiese *et al.* (2011), the primary goal is the confinement of short-periodic, long-wavelength AO components to the low-degree spectrum which in turn prevents them from manifesting as temporal aliasing effects, that is striping, within the long-term field's high-degree spectrum. The DMD is therefore primarily expected to facilitate, or rather to enhance, the retrieval of the full AOHIS signal. Alternatively, the background-model-based de-aliasing could also be applied to the observations before the DMD processing is engaged, thus allowing for a potentially enhanced retrieval of HIS.

In the following we explicitly discuss each step of this proposed processing scheme in order to identify which signal components are mapped into which part of the gravity spectrum, thereby disclosing its potential flaws and shortcomings.

In an initial step, observations (in the real GRACE-/GRACE-FO-case, these are ranges and/or range-rates) are accumulated based on a gravity signal up to some maximum spherical harmonic degree $n_{\max}$ (in the general case, $n_{\max} = \infty$). For the sake of simplicity, let us assume

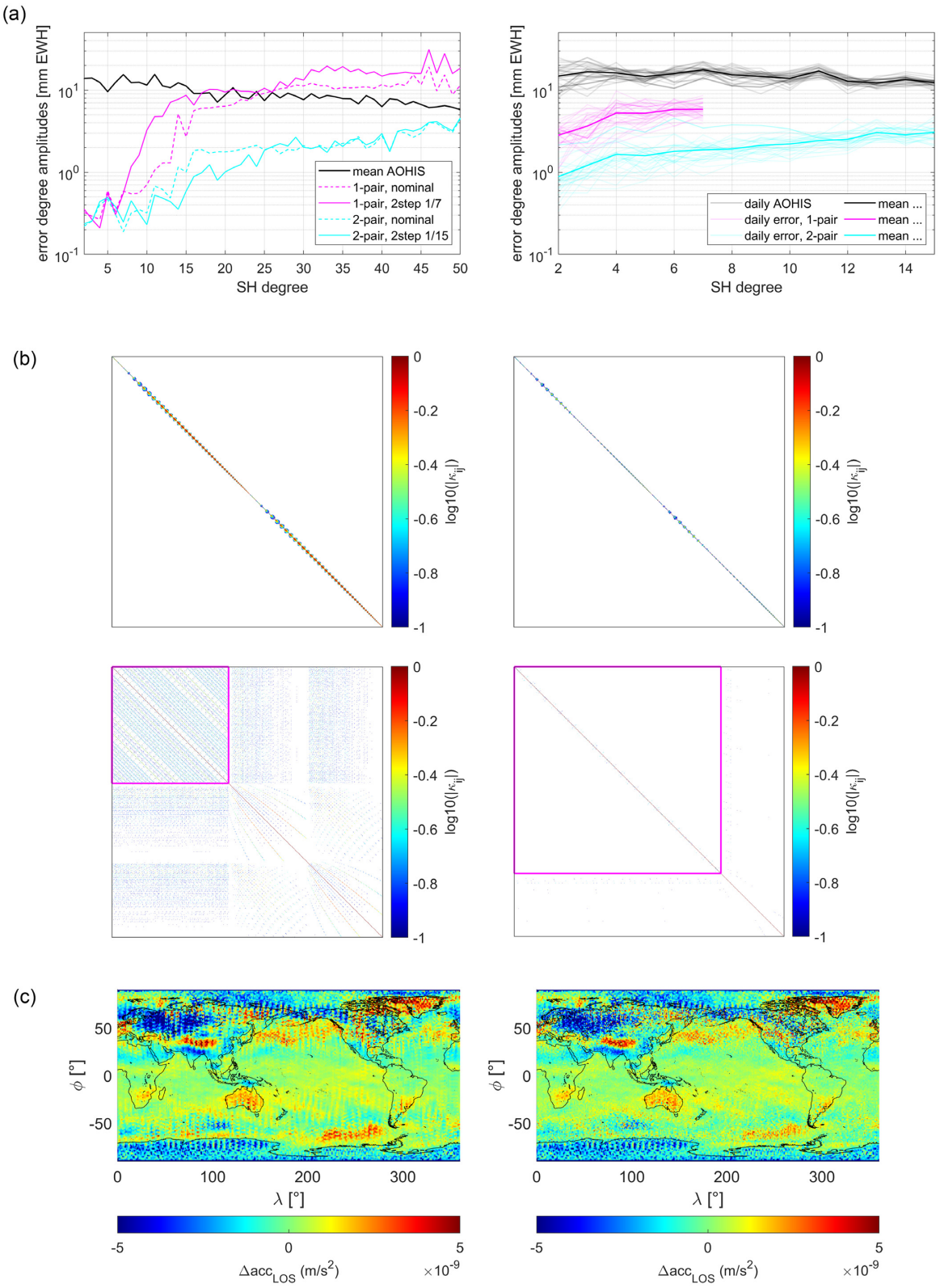

Figure 2. (a) shows the retrieval error of a 1- and 2-pair-based 30-d gravity solution where the full AOHIS signal is observed and the two-step co-parametrization and the nominal processing is applied (left) as well as the retrieval error of the corresponding co-estimated interval fields (right). (b) shows the correlation matrices of the estimated spherical harmonic coefficients for the four retrieval scenarios shown in (a)—1-pair, nominal (top left), 2-pair nominal (top right), 1-pair, 2-step (bottom left) and 2-pair, 2-step (bottom right)—on a logarithmic scale. The presented parameters are ordered first by short- and long-term, then by cos- and sin-coefficient, then by order, then by degree. Note that only correlation coefficients with an absolute value above 10 per cent are shown. The magenta boxes denote the 30 sets of daily parameters estimated up to the respective n_{int}. (c) shows the observations of the polar pair (left) as well as of the polar and the inclined pair (right) in terms of range accelerations interpolated on a global grid.

that this relation is of linear nature and can thus be written as

$$l = AX, \tag{1}$$

where l denotes the satellite pair's observations, X the Stokes' coefficients of the underlying gravity signal and A the functional relation between them. Note that in the general case where no signal periodicity can be assumed (which is true for the majority of short-periodic non-tidal signals), each observation carried out at any given time sample is based on an individual set of gravity field parameters. Thus, A, X and l can be written as

$$A = \begin{bmatrix} A_{I,1} & & & & & & & & 0 \\ & \dots & & & & & & & \\ & & A_{I,n} & & & & & & \\ & & & A_{II,1} & & & & & \\ & & & & \dots & & & & \\ & & & & & A_{II,n} & & & \\ & & & & & & \dots & & \\ & 0 & & & & & & \dots & \\ & & & & & & & & A_{N,n} \end{bmatrix}$$
$$X = \begin{bmatrix} X_{I,1} \dots X_{I,n} & X_{II,1} \dots X_{II,n} & \dots \dots X_{N,n} \end{bmatrix}^T \tag{2}$$
$$l = \begin{bmatrix} l_{I,1} \dots l_{I,n} & l_{II,1} \dots l_{II,n} & \dots \dots l_{N,n} \end{bmatrix}^T,$$

where $i = I, II, \dots N$ denotes a certain interval, for example 1 d, and $j = 1, 2, \dots n$ denotes the respective epoch, that is time sample, within the interval. The observations l can further be split into low- and high-degree-based components, that is ones which originate from the gravity spectrum up to n_{int} and upwards from $n_{\text{int}} + 1$, respectively. Consequently, (1) can be rewritten as

$$l = l_L + l_H = A_L X_L + A_H X_H, \tag{3}$$

where the indices L and H denote the signals related to the low- and high-degree spectrum.

The estimation of the low-resolution interval fields for a given interval i by means of least-squares adjustment then reads

$$\bar{x}_{i,L} = \left(a_{i,L}^T \Sigma_{l_i l_i}^{-1} a_{i,L}\right)^{-1} a_{I,L}^T \Sigma_{l_i l_i}^{-1} l_i = \left(a_{i,L}^T \Sigma_{l_i l_i}^{-1} a_{i,L}\right)^{-1} a_{I,L}^T \Sigma_{l_i l_i}^{-1} \left(A_{i,L} X_{i,L} + A_{i,H} X_{i,H}\right) \tag{4}$$

where

$$a_{i,L} = \begin{bmatrix} A_{i,1,L} \\ \dots \\ A_{i,n,L} \end{bmatrix} \tag{5}$$

and $\Sigma_{l_i l_i}$ is the covariance matrix representing the stochastic properties of the observations in the given interval. Note that in this representation the intervals are assumed to be entirely decoupled from one another, which in turn means that an optimal performance of the DMD can be expected if the underlying signals feature as few correlations between individual intervals as possible. Of course, more eloquent parametrization schemes based e.g. on weighted or unweighted moving windows could be applied in order to account for correlations between individual intervals, but such methods are not further investigated in the scope of this work.

The corresponding reference observations $\bar{l}_{i,L}$ to be used for the de-aliasing step then read

$$\bar{l}_{i,L} = a_{i,L}\, \bar{x}_{i,L}. \tag{6}$$

Evidently, they deviate from the true observations' low-degree-related components by

$$\Delta_i = \bar{l}_{i,L} - l_{i,L} = a_{i,L} \bar{x}_{i,L} - A_{i,L} X_{i,L} = C_{i,L} \left(A_{i,L} X_{i,L} + A_{i,H} X_{i,H}\right) - A_{i,L} X_{i,L} \tag{7}$$

with

$$C_{i,L} = a_{i,L} \left(a_{i,L}^T a_{i,L}\right)^{-1} a_{i,L}^T. \tag{8}$$

It is clear that Δ comprises two main effects. On one hand, spectral leakage is induced since components related to the high-degree spectrum are now mapped into the low degrees. On the other hand, an averaging error inevitably occurs since the observations of a given interval are now represented through a single set of Stokes' coefficients instead of through an individual set of coefficients at each time sample. In order to reduce the amplitude of Δ one should thus aim to first reduce high-degree signal components while simultaneously reducing the interval length. Using shorter time intervals is generally feasible, although lower-boundary limitations are dictated by the availability of a sufficient global observation coverage. As for the high-degree signal components, the by far largest contribution stems from the static field. Treating this component prior to the estimation of the interval fields is crucial, as otherwise the entirety of the corresponding signal would be parametrized into the low-degree spectrum, thus inducing a large-scale error that would greatly hamper the DMD approach. It is therefore suggested to either reduce the entire static signal from (3) based on a corresponding BM before estimating the interval fields, or to just reduce

its short-wavelength components and retain the low-degree part in (4). While the second approach is technically preferable since no modelling is required for the low-degree part, it can be shown that both approaches yield very similar results and that the imperfect knowledge of the true static field is secondary compared to the aliasing effects induced by the time-variable signals. It is also noted that the second approach is equivalent to the estimation of the interval fields up to $n_{\max}$ while fixing the high-degree spectrum to the static signal values. Further, a reduction of short-wavelength signals related to time-variable gravity might also be considered. However, this approach is not quite trivial and is also not further pursued in this work, although it may well be subject of future investigations.

Combining (6) and (1) to the reduction step then results in

$$l_i^{\text{red}} = l_i - \bar{l}_{i,L} = A_{i,H} X_{i,H} - \Delta_i. \tag{9}$$

Note that independently of the treatment chosen for the static signal, l_i^{red} does not include any static signal anymore except for the errors due to its imperfect reduction. Eq. (9) shows that the signal components which have been misparametrized in (4) are fully translated to the reduced observations and will thus affect the estimation of the reduced long-term solution y, which is computed as

$$y = y_L + y_H = \left(B^T \left(\Sigma_{l_i l_i} + \Sigma_{\bar{l}\bar{l}}\right)^{-1} B\right)^{-1} B^T \left(\Sigma_{l_i l_i} + \Sigma_{\bar{l}\bar{l}}\right)^{-1} l^{\text{red}} \tag{10}$$

with

$$B = \begin{bmatrix} A_{I,1} \\ \dots \\ A_{N,n} \end{bmatrix}, \quad \Sigma_{\bar{l}\bar{l}} = \begin{bmatrix} \Sigma_{\bar{l}_I \bar{l}_I} & & 0 \\ & \dots & \\ 0 & & \Sigma_{\bar{l}_N \bar{l}_N} \end{bmatrix}, \quad l^{\text{red}} = \begin{bmatrix} l_I^{\text{red}} \\ \dots \\ l_N^{\text{red}} \end{bmatrix}. \tag{11}$$

It is once again emphasized at this point that (10) is carried out for the entire spectrum, i.e. from d/o 0 up to $n_{\max}$, and not only for the higher-degree spectrum denoted as H in order to be able to obtain full co-variance information of y.

By substituting (9) and (7) into (10) we then obtain

$$y = D\, l^{\text{red}} = \underbrace{D \begin{bmatrix} A_{I,L} X_{I,L} + A_{I,H} X_{I,H} \\ \dots \\ A_{N,L} X_{N,L} + A_{N,H} X_{N,H} \end{bmatrix}}_{T1} \underbrace{- D \begin{bmatrix} C_{I,L} A_{I,L} X_{I,L} \\ \dots \\ C_{N,L} A_{N,L} X_{N,L} \end{bmatrix}}_{T2.1} \underbrace{- D \begin{bmatrix} C_{I,L} A_{I,H} X_{I,H} \\ \dots \\ C_{N,L} A_{N,H} X_{N,H} \end{bmatrix}}_{T3.1}, \tag{12}$$

where

$$D = \left(B^T B\right)^{-1} B^T. \tag{13}$$

In a final step, since the signal content featured in $\bar{l}_L$ was not considered within the estimation of the long-term solution, it must now be restored. This is done by adding the mean of all interval solutions to the low-degree spectrum of y. This step yields the final long-term solution Y which can be denoted as

$$Y = Y_L + Y_H \tag{14}$$

with

$$\begin{aligned} Y_L &= y_L + \tfrac{1}{N} \sum_{i=1}^{N} x_{i,L} = y_L + \underbrace{\frac{1}{N} \sum_{i=1}^{N} \left(a_{i,L}^T a_{i,L}\right)^{-1} \left(a_{i,L}^T A_{i,L} X_{i,L}\right)}_{T2.2} + \underbrace{\frac{1}{N} \sum_{i=1}^{N} \left(a_{i,L}^T a_{i,L}\right)^{-1} \left(a_{i,L}^T A_{i,H} X_{i,H}\right)}_{T3.2} \\ Y_H &= y_H \end{aligned} \tag{15}$$

After the static signal component is restored to either the entirety of Y or just to Y_H, depending on its previously chosen treatment, the DMD scheme is concluded. In an alternative approach, the interval fields' mean value can be computed in an additional step between (4) and (6) and already restored to (6) instead of (14), so that the reference observations used for the de-aliasing step in (9) are only comprised of variations with respect to the total signal's long-term mean. It can easily be shown that both approaches are equivalent and yield an identical result. Note that instead of a regular mean also a weighted mean of the interval fields can be employed where, e.g. the respective *a posteriori* variance factors may serve as weights. Such a procedure is of primary interest for real data processing since the impact of potential observation data gaps can be attenuated in this way.

In (12) the term $T1$ denotes the nominal parametrization scheme. The term $T2.1$ essentially represents the component responsible for the reduction of aliasing induced by low-degree-based signal components. Here it can clearly be seen that while a part of the low-degree-based signal is (correctly) prohibited from entering the high-degree spectrum, it is also reduced from the low degrees. To a large extent, this error is then counteracted by restoring the interval fields' mean to the long-term solution [*cf.* $T2.2$ in (15)]. The term $T3.1$ in eq. (12) represents an additional error which arises due to the presence of misparametrized high-degree components into the interval estimates (*cf.* eq. 4) and constitutes the largest contribution to the total error budget. However, also here the restoration of the interval fields' mean can to some extent minimize this error's impact at least in the low degrees ($T3.2$ in eq. 15). The presence of both terms results in the conclusion that the DMD will enhance the long-term solution's retrieval performance if the impact of the de-aliasing outweighs that of the leakage error.

Table 1. Orbit parameters.

Sat.	Altitude (km)	Inclination (°)	Rev./nodal day	Ascending node (°)	Mean anomaly difference (°)
p-A	475	89	457/30	0	-
p-B					1.674
i-A	475	70	439/29	0	-
i-B					1.674

Finally, it should be stated that the DMD approach is not limited to the treatment of a single interval length, but can in principle be refined by an infinite number of such before the estimation of the long-term field is carried out. In this way, if in a first step de-aliasing fields are computed up to a certain d/o n_{K_1} over an interval length of K_1, then the reduced observation time series obtained in (9) can be resubstituted into (4) in order to estimate additional de-aliasing fields up to a certain d/o n_{K_2} over an interval length of K_2, where $n_{K_2} > n_{K_1}$ and $K_2 > K_1$, before estimating the long-term solution. Each additional de-aliasing step will simultaneously represent a stand-alone gravity solution for the respective interval. However, the overall value for the estimation of the long-term field must be evaluated for each individual case, since additional errors (cf. eq. 7) are introduced with each additional iteration which may eventually outweigh the DMD's benefits.

4 DMD PERFORMANCE VALIDATION IN CLOSED-LOOP SIMULATIONS

In the following, the DMD's added value for the retrieval of time-variable gravity signals is evaluated within numerical closed-loop simulations. In Section 4.1, we give an overview over the simulation environment and the simulation parameters, while in Section 4.2 the single-pair-based simulation results obtained on the basis of various DMD schemes are presented. An outlook towards the applicability of DMD to Bender-type-based gravity retrieval is given in Section 4.3.

4.1. Simulation environment and parameters

The numerical closed-loop simulations are carried out with the IAPG's (Institute of Astronomical and Physical Geodesy) reduced-scale simulation software (RSS) in order to evaluate and quantify the added value of the DMD for the retrieval of time-variable gravity signals. In comparison to real GRACE-type data processing, the observations are given in terms of acceleration differences along the line of sight instead of ranges or range-rates:

$$\Delta \mathrm{acc}_{\mathrm{LOS}} = \langle \Delta a_{\mathrm{grav}}, \Delta r_{\mathrm{LOS}} \rangle + \langle \Delta a_{\mathrm{non\text{-}grav}}, \Delta r_{\mathrm{LOS}} \rangle. \tag{16}$$

In the equation above, Δa_{grav} and $\Delta a_{\mathrm{non\text{-}grav}}$ represent the differences in gravitational and non-gravitational acceleration observed by the satellites of one pair in along-track, cross-track and radial directions, respectively, while Δr_{LOS} denotes the vector between their centres of mass. In this case, the gravity field adjustment turns into a linear problem, thus greatly reducing the required computational effort. For a detailed description of the RSS the reader is referred to Murböck (2015) and Murböck *et al.* (2014).

In this study, repeat orbits whose parameters are denoted in Table 1 are used for both the polar as well as for the inclined satellite pair. For the static gravity signal, we employ the model GOCO06s (Kvas *et al.* 2019; Kvas *et al.* 2021). In order to account for the uncertainty with which the static field is known, the retrieval step is carried out with GOCO06s superimposed with an error which is derived from the full covariance matrix of the estimated SH coefficients provided along with the model itself. The OT de-aliasing error is introduced through the difference of the models GOT4.7 (successive update to Ray 1999) and EOT11a (Savchenko & Bosch 2012) where we consider contributions of the eight principal tidal constituents. We further consider sensor noise contributions to the total error budget. Here, we take into account only the two most dominant components—the accelerometer and the ranging instrument. For the former, we assume an NGGM-type error behaviour derived from Pail *et al.* 2018 according to

$$d_{\mathrm{acc},X} = d_{\mathrm{acc},Z} = 10^{-11} \sqrt{\left(\frac{10^{-3}\mathrm{Hz}}{f}\right)^2 / \left(\left(\frac{10^{-5}\mathrm{Hz}}{f}\right)^2 + 1\right) + 1 + \left(\frac{f}{10^{-1}\mathrm{Hz}}\right)^2} \left[\frac{m}{s^2\sqrt{\mathrm{Hz}}}\right] \quad d_{\mathrm{acc},Y} = 10 \cdot d_{\mathrm{acc},X} \tag{17}$$

with X denoting measurements in the along-track, Y in the cross-track and Z in the radial direction, while for the latter we assume a laser ranging interferometer with a noise performance according to

$$d_{\mathrm{LRI}} = 4 \cdot 10^{-8} \sqrt{\left(\frac{10^{-2}\mathrm{Hz}}{f}\right)^2 + 1} \left[\frac{m}{\sqrt{\mathrm{Hz}}}\right], \tag{18}$$

cf. Iran Pour *et al.* (2015). With regard to the accelerometer, it is noted that the satellites are assumed to be perfectly aligned along their line of sight, so the cross-track and radial axes do not contribute to the total error budget. The primary focus of this study lies on the retrieval of non-tidal temporal gravity variations which are introduced into the simulation environment through the AOHIS fields taken from the Updated ESA Earth System Model (Dobslaw *et al.* 2014). An overall retrieval period of 30 d is investigated in this study, for which we estimate a

gravity solution up to d/o 96 (which is one of the standard resolutions of the monthly GRACE products). In order to maintain full consistency with the chosen retrieval resolution and in this way to create an optimal environment for testing the DMD approach, all underlying gravity signals are also truncated at d/o 96.

The retrieval performance of a given simulation scenario is then evaluated based on the retrieved solution's deviation to the true signal which is presented in terms of degree amplitudes rescaled to equivalent water heights according to

$$c_{n,amp} = \frac{R}{3} \cdot \frac{\rho_{av}}{\rho_w} \cdot \frac{2n+1}{1+k'_n} \sqrt{\sum_{m=0}^{n} \Delta\bar{C}^2_{nm} + \Delta\bar{S}^2_{nm}} \; [m], \tag{19}$$

where $\Delta\bar{C}^2_{nm}$ and $\Delta\bar{S}^2_{nm}$ are the underlying Stokes' coefficients, R is the Earth radius, ρ_{av} and ρ_w denote the average density of the Earth and that of water, respectively, and k'_n are the second load love numbers. Further, for the sake of an easy comparison between the various simulation scenarios, selected results are also summarized in Table 2 in terms of the root mean square (RMS) of latitude-weighted global equivalent water height (EWH) error grids (i.e. the grid points are scaled with the cosine of their latitude) for various spatial resolutions. The table is provided at the end of Section 4.

4.2. Single-pair simulation results

4.2.1. Regular DMD

In a first set of simulations, the DMD is applied to the non-tidal time-variable gravity signal according to the approach presented in Section 3 and its impact on the retrieval performance is studied. We thus assume that the satellites' observations are based solely on the AOHIS signal components while all other error contributors are disregarded (in case of the static field we assume that it is perfectly known). The retrieval is carried out based on the nominal processing strategy as well as on the DMD approach, for which daily de-aliasing fields are estimated up to d/o 7, 12 and 15. The first scenario is chosen because the orbit configuration at hand allows for a numerically stable solution up to d/o 7 from one day of observations according to the Nyquist-Colombo theorem (Colombo 1984). However, Weigelt *et al.* (2013) have shown that this rule of thumb is too conservative for a near-polar orbit in case of an odd parity of $\beta - \alpha$, where β denotes the integer number of revolutions within a repeat period and α the integer duration of the latter in days. According to this study, the limitation is related to the spherical harmonic order rather than to the degree and reads $m < \beta$ if $\beta - \alpha$ is odd and $m < \frac{\beta}{2}$ if it is even, m being the maximum resolvable order. Since an odd parity of $\beta - \alpha$ is given in the configuration at hand (*cf.* Table 1), a 1-d solution up to max. d/o 12 can be considered achievable, while d/o 15 is just out of range. Nevertheless, because d/o 15 has been shown to be the optimal resolution for the two-step co-parametrization approach in case of a Bender-type retrieval and because the primary focus is put on the performance of the long-term solution rather than on that of the interval ones, this scenario is also investigated.

The results are presented in Fig. 3(a). It shows that the DMD's improved parametrization is indeed capable of reducing the temporal aliasing in the higher spherical harmonic degrees, and that this effect increases with a larger maximum resolution of the de-aliasing fields. Thus, a maximum improvement of up to 80 per cent can be achieved in the spectrum above d/o 15 with DMD 1/15[1] in comparison to the nominal processing, while DMD 1/7 only yields a maximum improvement of 40 per cent. Conversely, it also becomes evident that the DMD approach degrades the retrieval of the low-degree spectrum, where the level of degradation is evidently proportional to the maximum resolution of the interval fields. This additional error is still negligible in case of DMD 1/7 and DMD 1/12 (since the signal-to-noise ratio (SNR) is below 1), but in case of DMD 1/15 it begins to dominate the monthly gravity solution in certain spectral bands (e.g. below d/o 6 and around d/o 15).

In order to better understand the reason for this behaviour, the AOHIS signal is split up into the AO and the HIS components and the previous simulation scenarios are repeated. In case of AO-only, *cf.* Fig. 3(b), the retrieval error obtained with the nominal processing remains practically unchanged in comparison to the one obtained in the case of AOHIS, which means that the overall retrieval performance of AOHIS is dictated by the AO-induced aliasing. Once the DMD is applied, one can once again observe a deterioration within the low degrees, while the retrieval performance above d/o 15 is identical to the full-AOHIS scenario. The degradation in the low-degree spectrum, however, now features lower amplitudes than in the case of AOHIS, on average by a factor of 3. It can thus be concluded that the performance within the long-wavelength spectrum must be significantly influenced by HIS, which can fully be confirmed by the results shown in Fig. 3(c). Here it can be seen that while in case of the nominal processing the HIS-contributions to the total retrieval error are negligible next to the AO aliasing, the monthly fields' low-degree spectrum is indeed—at least partially—dominated by the HIS once the DMD is applied. It is notable that the DMD leads to a significantly decreased retrieval performance in comparison to the nominal processing by several orders of magnitude below d/o 10 in all investigated scenarios. This deterioration persists up to d/o 50, whereas from this SH degree onwards the DMD once again yields an improved solution quality by up to 50 per cent in case of DMD 1/7 and up to 80 per cent in case of DMD 1/15.

In order to fully reveal the reason for the improvements and the degradations related to the DMD approach, an additional set of simulations is carried out where the input signal's spectral content above d/o n_{int} or below d/o $n_{int} + 1$ (n_{int} being the maximum resolution

[1]The nomenclature DMD *x*/*y* denotes that de-aliasing fields are estimated up to a maximum d/o *y* at intervals of *x* days within the DMD processing scheme.

Table 2. Retrieval performance of selected simulation scenarios under application of various DMD schemes in terms of (latitude-weighted) RMS of global EWH grids synthesized up to maximum d/o 20, 40, 60 and 96. The values are given in (mm EWH).

Mission type	**Target signal** and further error contributors	Processing strategy	Constraint applied	$n = 20$	$n = 40$	$n = 60$	$n = 96$
1-pair	**AOHIS**	nominal	-	45.4	94.5	272.1	5637.2
		DMD 1/7	No	21.4	47.2	212.5	4123.7
		DMD 1/20	No	27.7	39.9	137.8	2412.0
		DMD 1/15	No	63.2	69.6	120.8	1863.6
		DMD 1/7	Yes	21.4	47.2	212.0	4127.1
		DMD 1/20	Yes	17.3	33.5	136.0	2405.2
		DMD 1/15	Yes	12.9	31.1	101.7	1853.5
		DMD 1/7, 2/20	No	21.0	45.8	134.1	1497.2
		DMD 1/12, 2/20	No	29.4	42.2	111.2	1405.8
		DMD 1/15, 2/25	No	70.3	81.1	120.7	948.7
		DMD 1/7, 2/20	Yes	14.2	43.0	132.6	1504.6
		DMD 1/12, 2/20	Yes	12.3	33.0	106.1	1391.3
		DMD 1/15, 2/25	Yes	9.2	31.9	91.6	935.9
	AOHIS, OTD, static field, instruments	Nominal	-	10.7	70.8	297.0	5933.9
		DMD 1/7, 2/20	Yes	14.4	43.1	143.7	1565.0
		DMD 1/12, 2/20	Yes	13.0	33.7	115.3	1475.1
		DMD 1/15, 2/25	Yes	11.0	32.6	102.7	1037.4
	HIS, AOD, OTD, static field, instruments	Nominal	-	6.1	16.2	104.4	1328.0
		DMD 1/7, 2/20	Yes	11.9	28.6	58.7	518.9
		DMD 1/12, 2/20	Yes	12.4	28.1	57.0	531.2
		DMD 1/15, 2/25	Yes	9.0	28.6	57.2	452.7
2-pair	**AOHIS**, OTD, static field, instruments	Nominal	-	5.4	12.4	44.4	426.5
		2-step 1/15	-	3.8	13.1	36.0	334.3
		DMD 1/15	No	4.4	12.8	33.0	293.5
		DMD 1/20, 2/40	No	5.2	18.7	33.3	196.5
		DMD 1/15, 2/30, 3/45	No	4.6	15.2	32.0	207.6
		DMD 1/15	Yes	4.3	12.8	33.0	293.4
		DMD 1/20, 2/40	Yes	4.2	11.7	29.7	196.7
		DMD 1/15, 2/30, 3/45	Yes	3.9	11.9	29.3	207.5
	HIS, AOD, OTD, static field, instruments	Nominal	-	4.8	7.9	21.0	178.8
		2-step 1/15	-	5.7	8.5	21.0	180.1
		DMD 1/15	No	7.0	11.7	21.2	155.1
		DMD 1/20, 2/40	No	6.5	16.6	28.7	129.0
		DMD 1/15, 2/30, 3/45	No	6.3	14.5	25.7	137.8
		DMD 1/15	Yes	7.0	11.7	21.2	155.1
		DMD 1/20, 2/40	Yes	5.7	10.1	25.3	128.8
		DMD 1/15, 2/30, 3/45	Yes	5.8	11.3	22.9	137.0

of the DMD's interval fields), respectively, is removed. As a reference, we use the nominal processing scheme for which the input signal is truncated in the same way.

In case of AO-only, *cf.* Fig. 4(b), left, the retrieval performance varies only minimally between the different scenarios in case of the nominal processing. In contrast, in case of the DMD all scenarios yield a significant aliasing reduction of low-degree-based signal components above the respective n_{int} by up to one order of magnitude. At the same time, the solution quality deteriorates notably below n_{int} in case of DMD 1/12 and even more severely in case of DMD 1/15. This effect cannot arise from the leakage of high-degree components into the short-wavelength spectrum since no high-degree signal is present, and it also cannot be caused by the effect previously denoted as the averaging error in Section 3 (*cf.* eq. 8), because it affects all DMD scenarios in the same manner. The only remaining explanation is therefore

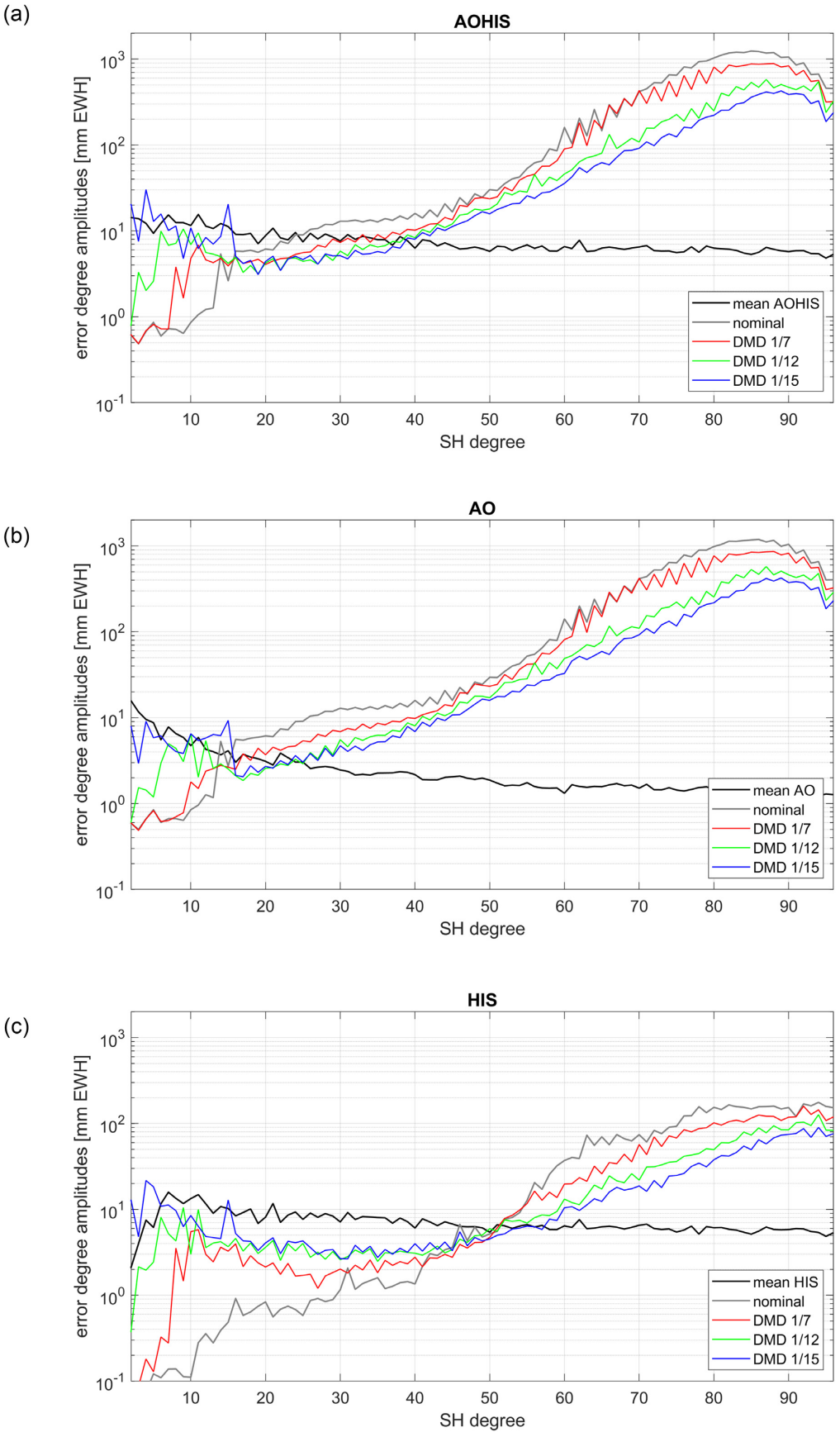

Figure 3. Retrieval error of the 1-pair-based 30-d solutions based on the full AOHIS (a), AO (b) and HIS (c) signal under employment of the nominal processing as well as of various single-period DMD schemes.

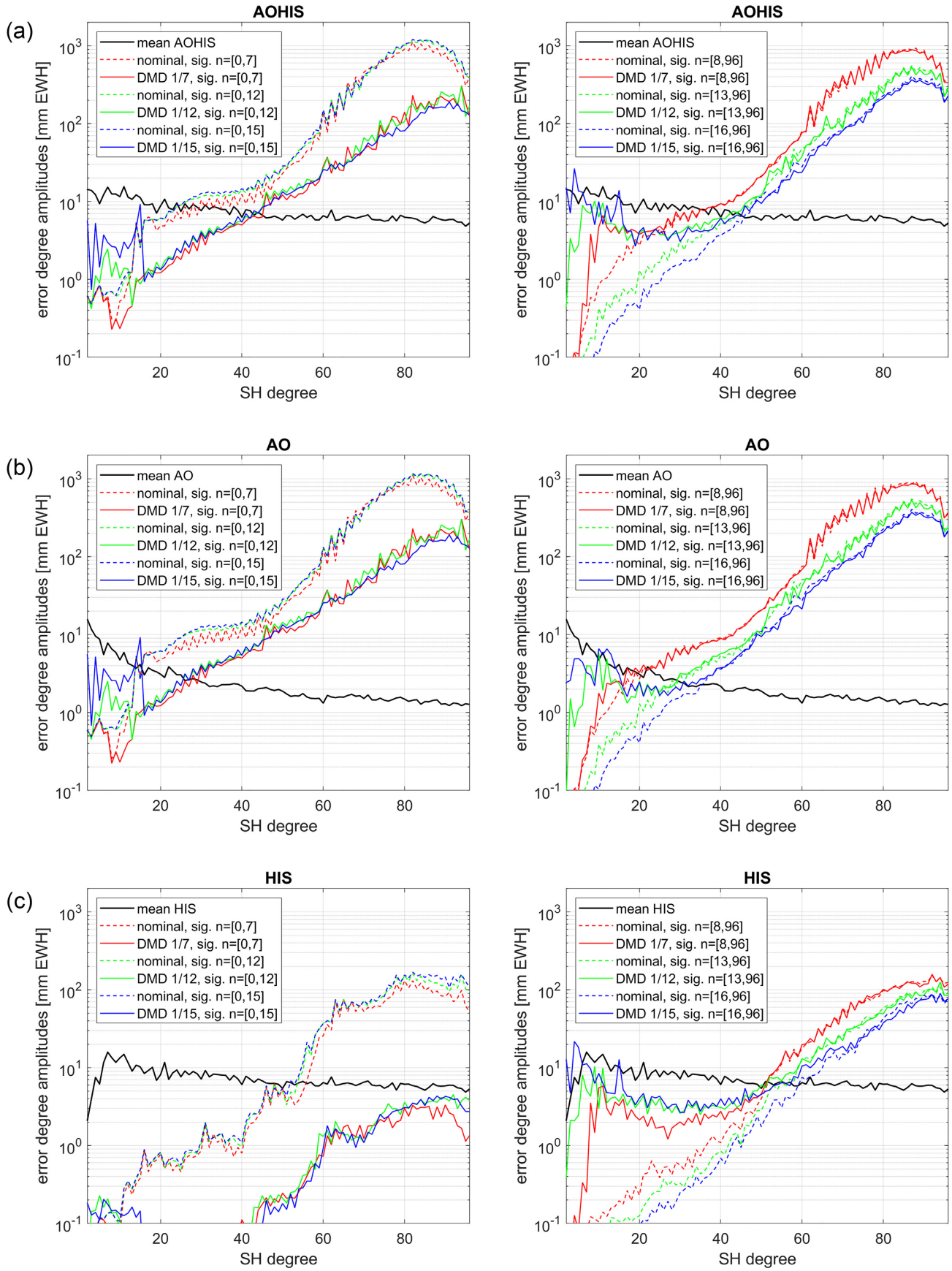

Figure 4. Retrieval error of the 1-pair-based 30-d solutions based on the full AOHIS (a), AO (b) and HIS (c) signal under employment of various single-period DMD schemes. In the plots on the left-hand side, the signals related to the spectral bands up to the respective n_{int} have been set to zero while in the plots on the right-hand side, the signals related to the spectral bands upwards from the respective $n_{int} + 1$ have been set to zero.

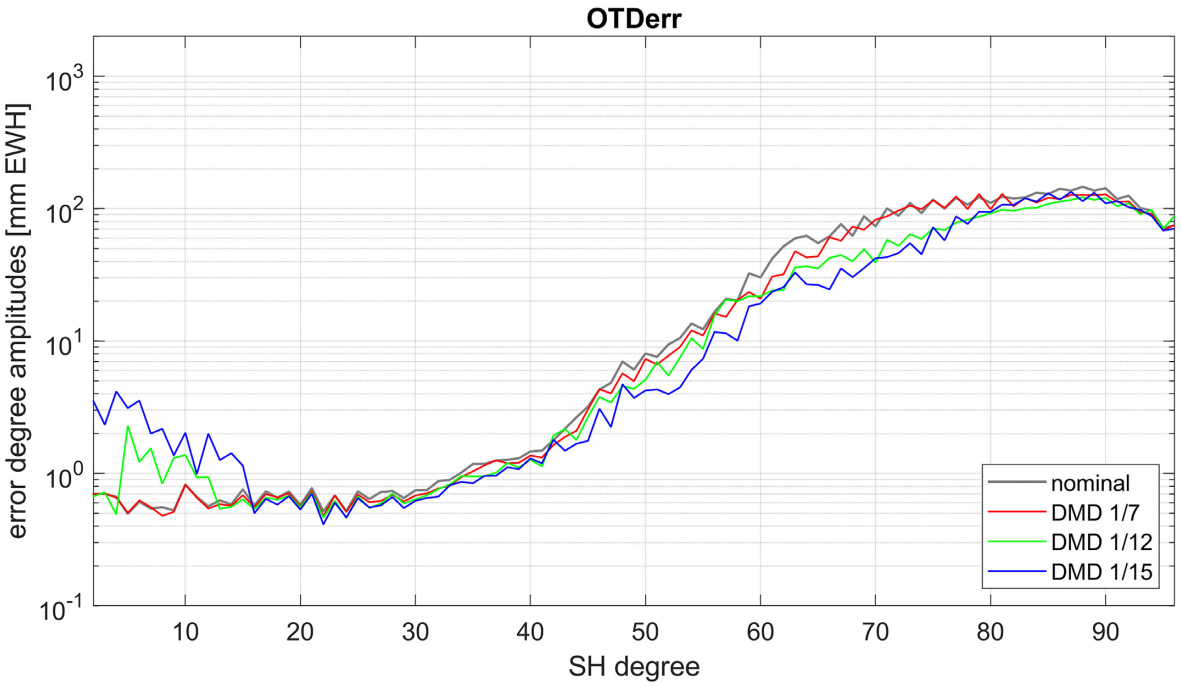

Figure 5. Retrieval error of the 1-pair-based 30-d solutions based on the residual OT signal (after application of BM-based de-aliasing) under employment of various single-period DMD schemes.

the single pair's insufficient spatial resolution. This assumption is further supported by the fact that no degradation occurs in case of DMD 1/7, as 7 is the maximum resolvable degree according to the Nyquist-Colombo theorem.

Fig. 4(b), right, shows the processing strategies' impact on the high-degree-based AO components. One can establish that the nominal processing's performance improves with increasing n_{int}. This behaviour is logical, since a lower amount of misparametrization can occur when less signal is present. In contrast, in case of DMD a higher n_{int} leads to additional degradations in the low-degree spectrum, while the high degrees remain almost unaffected compared to the nominal processing method. This effect can be fully attributed to the spectral leakage (*cf.* $T3.1$ and $T3.2$ in eqs 12 and 15), since the processing explicitly attempts to capture high-degree signal within the low degrees. Evidently, the higher n_{int} is set, the more signal is also irreversibly misparametrized.

An analogous investigation of the HIS components, *cf.* Fig. 4(c), reveals a very similar overall behaviour as the previously discussed AO scenarios, although the aliasing of low-degree-based signal components is notably smaller while, adversely, the leakage-induced degradation of the low-degree retrieval performance is notably larger in comparison to the nominal processing. This behaviour can be attributed to the fact that the strongest HIS signals occur on medium to short spatial wavelengths. Therefore, any misparametrization related to this part of the spectrum has a strong effect on the retrieval quality. Vice versa, the dominant AO signal components can be found in the low spatial frequencies, so the effect of misparametrizations of the higher-degree signal is less pronounced. In case of AOHIS, *cf.* Fig. 4(a), the effects of AO and HIS are combined, and the total retrieval performance in a given spectral band is dictated by the individual errors of each of the two sets of constituents. In this way, the degradation in the monthly solution's low degrees is predominantly related to the leakage of high-degree HIS signal components, while the improvements in its higher degrees are attributed to the combined effect of reduced low- and high-degree-based AO signals' aliasing.

For the sake of completeness, we also investigate the DMD's impact on the OT signal. The results presented in Fig. 5 indicate a similar behaviour as in case of the non-tidal variations. Thus, DMD 1/7 improves the retrieval performance in the spectrum around d/o 60 (up to 30 per cent improvement compared to the nominal case) without notably affecting the low degrees. In contrast, the cases DMD 1/12 and 1/15 lead to stronger degradations in the long wavelengths (up to a factor 4 in case of DMD 1/15) while simultaneously yielding larger improvements in the high-degree spectrum (up to 60 per cent in case of DMD 1/15). However, it can clearly be seen that the imperfect OT de-aliasing's total error contribution is entirely subordinate to that of the AO signal when comparing the amplitudes of the respective retrieval errors, and is thus of secondary interest for the moment.

4.2.2. Constrained DMD

In conclusion, the DMD can be regarded as a trade-off between an improved retrieval performance within the short wavelengths at the cost of a reduced solution quality in long-wavelength spectrum. While, of course, undesirable, the degradation within the low degrees can be tolerated as long as the overall SNR remains below the value of 1, as is e.g. the case for DMD 1/12. However, while in a simulation environment both the true signal and the uncertainty with which it is retrieved are known, the true SNR can only be vaguely approximated in case of real data

processing. It is therefore essential to reduce the level of deterioration within the low-degree spectrum as far as possible in order to minimize its potential impact on the gravity retrieval. We attempt to achieve this goal by applying an additional constraint to the processing scheme which fixes the mean of the interval fields to the corresponding spectrum of the nominal solution, i.e.

$$\frac{1}{N}\sum_{i=I}^{N}\begin{Bmatrix}C_{nm}\\S_{nm}\end{Bmatrix}_i=\begin{Bmatrix}C_{nm}\\S_{nm}\end{Bmatrix}_{\bar{X}};n=0,\dots n_{int},\ m=0,\dots n \tag{20}$$

where N is the number of individual interval solutions, i once again denotes the interval and $\bar{X}$ denotes the nominal solution obtained according to

$$\bar{X}=\left(diag(A)^T\Sigma_{ll}^{-1}diag(A)\right)^{-1}diag(A)^T\Sigma_{ll}^{-1}l, \tag{21}$$

with A taken from (2). It is emphasized that it is essential to retain the interval fields' mean within (6) in case the constraint is applied, since its reduction would induce a mismatch between the interval fields and the nominal solution. Further, it is noted that (20) implies the application of an unweighted mean of the interval fields. However, a weighted mean which allows for a consideration of prior knowledge about the performance of the estimated interval fields, e.g. related to data gaps or similar issues, can also be applied. The constraint itself is introduced in terms of pseudo-observations within the estimation of the interval fields $\bar{x}_{i,L}$ which alters Eq. (4) to

$$\begin{bmatrix}\bar{x}_{I,L}\\\dots\\\bar{x}_{N,L}\end{bmatrix}=\left(F^T\Sigma_{l_cl_c}^{-1}F\right)^{-1}\left(F^T\Sigma_{l_cl_c}^{-1}\begin{bmatrix}l_I\\\dots\\l_N\\\bar{X}_L\end{bmatrix}\right)=\left(F^T\Sigma_{l_cl_c}^{-1}F\right)^{-1}\left(F^T\Sigma_{l_cl_c}^{-1}\begin{bmatrix}A_{I,L}X_{I,L}+A_{I,H}X_{I,H}\\\dots\\A_{N,L}X_{N,L}+A_{N,H}X_{N,H}\\\bar{X}_L\end{bmatrix}\right) \tag{22}$$

with

$$F=\begin{bmatrix}a_{I,L}&&0\\0&\dots&a_{N,L}\\\frac{1}{N}&\frac{1}{N}&\frac{1}{N}\end{bmatrix},\ \Sigma_{l_cl_c}=\begin{bmatrix}\Sigma_{ll}&0\\0&\Sigma_{\bar{X}_L\bar{X}_L}\end{bmatrix}, \tag{23}$$

where $a_{i,L}$ is set up according to (5), Σ_{ll} is the error variance-co-variance matrix (VCM) of observations and $\Sigma_{\bar{X}_L\bar{X}_L}$ is the error VCM of the nominal solution's low-degree spectrum, which may be scaled in order to regulate the constraint's overall impact. The magnitude of the scaling factor depends on the relative differences between Σ_{ll} and $\Sigma_{\bar{X}_L\bar{X}_L}$, and must therefore be determined individually for each processing scenario. Alternatively, $\Sigma_{\bar{X}_L\bar{X}_L}$ may also be set up e.g. as a scaled unity matrix, although this approach has been shown to generally yield results of overall lower quality in comparison. It is evident that contrary to the nominal DMD approach presented in Section 3, the constrained DMD does not allow for a separate processing of individual interval solutions anymore, thus somewhat increasing the computational demands.

A comparison of the retrieval errors obtained through the constrained and the unconstrained DMD in case of the full AOHIS signal, *cf.* Fig. 6(a), reveals a practically unchanged performance for DMD 1/7. However, this was to be expected, since the low-degree spectrum of the unconstrained DMD 1/7 solution already performed close to identically to that of the nominal solution. The constraint's immense added value is revealed once the interval fields' resolution is increased. In this way, the monthly solution's low-degree retrieval performance can be improved by up to an order of magnitude in case of DMD 1/12 and by up to 1.5 orders of magnitude in case of DMD 1/15 in case of the full AOHIS signal. While in this way the DMD-induced deterioration in the low-degree spectrum cannot be prevented entirely, it is nevertheless reduced to a level which can be deemed acceptable. It is further ideal that applying the constraint seems to affect almost exclusively the low-degree spectrum while the spectral bands above n_{int} remain nearly unchanged. Evidently, the additional information introduced by the constraint allows for an enhanced mapping of individual signal components within the interval fields, i.e. more low-degree-based signal components are correctly parametrized into the de-aliasing fields while simultaneously, less high-degree-based components are misparametrized. This is clearly confirmed by Fig. 6(b) and (c), where we once again explicitly demonstrate the individual error contribution of signals stemming from different spectral bands. Here, it is quite remarkable that the improvements are predominantly related to the prevention of erroneous parametrization of high-degree based components to the low-degree spectrum (i.e. to the interval solutions). It can be shown that this effect results in a retrieval quality enhancement by up to two orders of magnitude in the low degrees, while, in comparison, the improved parametrization of low-degree components yields an additional gain of a factor 2 to 3 (*cf.* Fig. 6b).

The constraint's added value can also be clearly seen in the corresponding interval fields. Here, its overall benefit also becomes more prominent with increasing n_{int}. As shown in Fig. 6(c), the interval fields' average uncertainty is reduced by up to 25 per cent in case of DMD 1/7 and by up to 50 per cent in case of DMD 1/12, while in case of DMD 1/15 the error reduction constitutes up to 70 per cent in comparison to the respective regular DMD scenario. The constraint is of special value for DMD 1/15, as it allows for the interval solutions to be retrieved with sufficient accuracy on average up to d/o 7, while in case of the unconstrained equivalent a reliable estimation is barely feasible up to d/o 3.

4.2.3. Multi-period DMD

In the following, we evaluate the benefit of subsequently estimating de-aliasing products at progressively longer intervals with an increasing spatial resolution. As already mentioned in Section 3, the DMD scheme is not limited to the estimation of de-aliasing fields at a single interval,

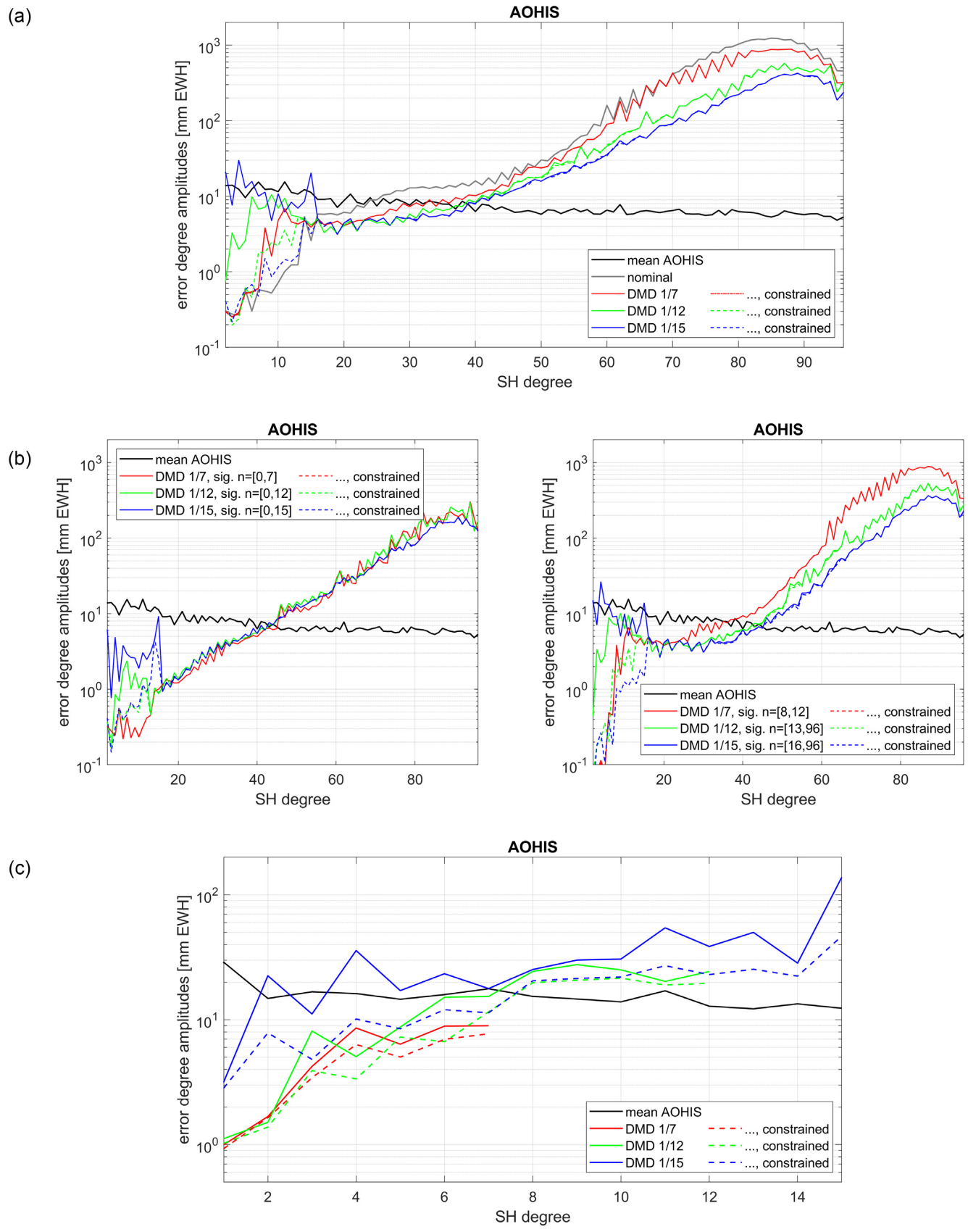

Figure 6. (a) Retrieval error of the 1-pair-based 30-d solutions based on the full AOHIS signal under employment of various constrained and unconstrained single-period DMD schemes. (b) Retrieval error of the 1-pair-based 30-d solutions under employment of the DMD schemes in a) where the underlying AOHIS signal components related to the spectral bands above the respective n_{int} (left) and below the respective $n_{\mathrm{int}} + 1$ (right) have been set to zero. (c) Mean retrieval error of the interval fields obtained with the DMD schemes used in (a).

but can in principle be extended by an infinite number of additional intermediate steps before the estimation of the final monthly product. In this way, one may reduce the impact of temporal aliasing for each subsequent iteration by capturing the inducing signal components within the interval fields. A potential drawback of this approach is the fact that with any additional iteration the DMD's naturally occurring errors (*cf.* eq. 7) simultaneously increase, which eventually might outweigh the DMD's de-aliasing capabilities within the long(er)-term solution(s).

As an example, we investigate the value of extending the previously evaluated scenarios DMD 1/7, DMD 1/12 and DMD 1/15 with an estimation of interval fields over a 2-d period. For DMD 1/7 and DMD 1/12 these are estimated up to d/o 20 (denoted as DMD 1/7, 2/20 and DMD 1/12, 2/20, respectively), while for DMD 1/15 the additional solutions are set up to d/o 25 (denoted as DMD 1/15, 2/25). The results presented in Fig. 7(a) where the performance of the regular DMD scenarios is compared against that of the multi-period ones indicate that the low-degree spectrum remains for the most part unaffected in case of DMD 1/7, 2/20 and DMD 1/12, 2/20 in comparison to the respective single-period approach. Notable degradations occur only below d/o 7 for DMD 1/7, 2/20 and below d/o 5 for DMD 1/12, 2/20. For DMD 1/15, 2/25, on the other hand, the retrieval performance is significantly deteriorated between d/o 15 and 25 in comparison to DMD 1/15. The added value of the multi-period estimation first becomes notable in the higher-degree spectrum (around d/o 25 for DMD 1/7, 2/20, d/o 30 for DMD 1/12, 2/20 and d/o 40 for DMD 1/15, 2/25) and continuously increases with higher spatial resolution. This way, a maximum improvement of *ca.* 70 per cent can be achieved with DMD 1/7, 2/20 and *ca.* 40 per cent with DMD 1/12, 2/20 and DMD 1/15, 2/20 with respect to the corresponding single-period estimation scenario.

Further, we evaluate the benefit of constraining the multi-period DMD analogously to the procedure shown above for the single-period DMD. Just like the DMD itself, the constraint is not limited to a single de-aliasing step, but can be applied at each iteration. In the example at hand, both the daily and the two-daily solutions are constrained up to their respective maximum degree of resolution. The results shown in Fig. 7(b) indicate that some additional gains can be achieved primarily between d/o 7 to 15 with the constrained multi-period processing scheme in comparison to the respective single-period approach. In all investigated cases, the retrieval performance in this spectral band can be improved by up to 30 per cent in this spectral range. Analogously to the results presented earlier, the constraint does not notably affect the spectrum above the maximum constrained spherical harmonic degree.

The constrained multi-period DMD scheme is thus without a doubt of great value for the retrieval of the monthly gravity product. At the same time, however, it also leads to a degradation of the interval fields estimated after the retrieval of the initial daily solutions. This can be seen in Fig. 7(c) where we compare the two-daily solutions obtained through the constrained DMD 2/20 and DMD 2/25 single-period schemes with their equivalents obtained with the previously discussed constrained multi-period DMD schemes. It can be seen that while the d/o 20 interval fields retrieved with the DMD 1/7, 2/20 feature an overall quite similar behaviour as their DMD 2/20 counterparts, those retrieved with DMD 1/12, 2/20 perform notably worse between d/o 5 and 12. Here, a degradation of up to a factor of 3 can be established. On the other hand, some improvements can also be found in the spectrum upwards from d/o 13. An overall similar relative behaviour can be established in the d/o 25 interval solutions obtained with DMD 2/25 and DMD 1/15, 2/25. It can thus be stated that the sum of misparametrization errors made within an estimation step of the DMD directly translates into the following one. The larger these misparametrization errors are, the higher also the uncertainty of the fields estimated in the subsequent step. Since aliasing-related errors generally feature lower amplitudes within a short-term gravity solution than in a field obtained from a longer observation period due to the maximum achievable spatial resolution (i.e. no striping can yet occur), these errors then outweigh the added value of aliasing reduction. Following this train of thought and taking into account the fact that the monthly estimate is in essence nothing other than an interval solution itself, it can be stated that once the intermediate retrieval intervals are increased to the point where the aliasing effects start to become dominant, the behaviour can be expected to reverse. Additional studies may be carried out in the future to identify this point of equilibrium and to further enhance the performance of the interval estimates. For now, the recommendation to apply multi-period DMD schemes in order to obtain the best-possible long-term estimate is given, while the results of intermediate interval steps should be treated with some reservations.

4.2.4. Application of DMD in full-noise scenario

For the sake of completeness, we also evaluate the DMD in a full-noise scenario where in addition to the full AOHIS signal we also consider the OT de-aliasing error as well as instrument noise and an error for the knowledge of the static field. Here, we only investigate the constrained multi-period DMD schemes, as these have been shown to yield the best overall results.

Since the temporal aliasing effects induced by the AO signal components are by far the most dominant error contributor, the DMD features a near-identical behaviour as in the case of AOHIS-only, as can clearly be seen in Fig. 8(a). The only notable deviations to this scenario can be found in the spectrum below d/o 10 which is heavily influenced by the OT signal as well as to a minor extent by the sensor noise. However, similarly to the AOHIS-only scenario, also in the full-noise case the constraint once again seems to almost entirely prevent any potential degradations in the low-degree spectrum. The full AOHIS signal can thus reliably be retrieved up to d/o 40 with the investigated DMD schemes, while in case of the nominal processing the retrieval is only possible up to d/o 25.

The DMD's overall value within the scope of self-de-aliasing of AO-based signal components is thus clearly demonstrated. As a final demonstration, we now abandon the attempt of retrieving the full AOHIS signal and instead focus exclusively on retrieving the HIS components by introducing prior BM-based de-aliasing of the AO components. In a reasonable approximation, this is achieved by downscaling the AO components' amplitudes by 90 per cent (H. Dobslaw, personal communication, 2021). Thus, the AO's error contributions still remain notable throughout the spectrum up to d/o 60, but allow for an overall stronger impact of OT de-aliasing errors (primarily up to d/o 50) and especially of the HIS's naturally occurring aliasing (dominant error contributor from around d/o 40 upwards) to the monthly solution. The impact of the

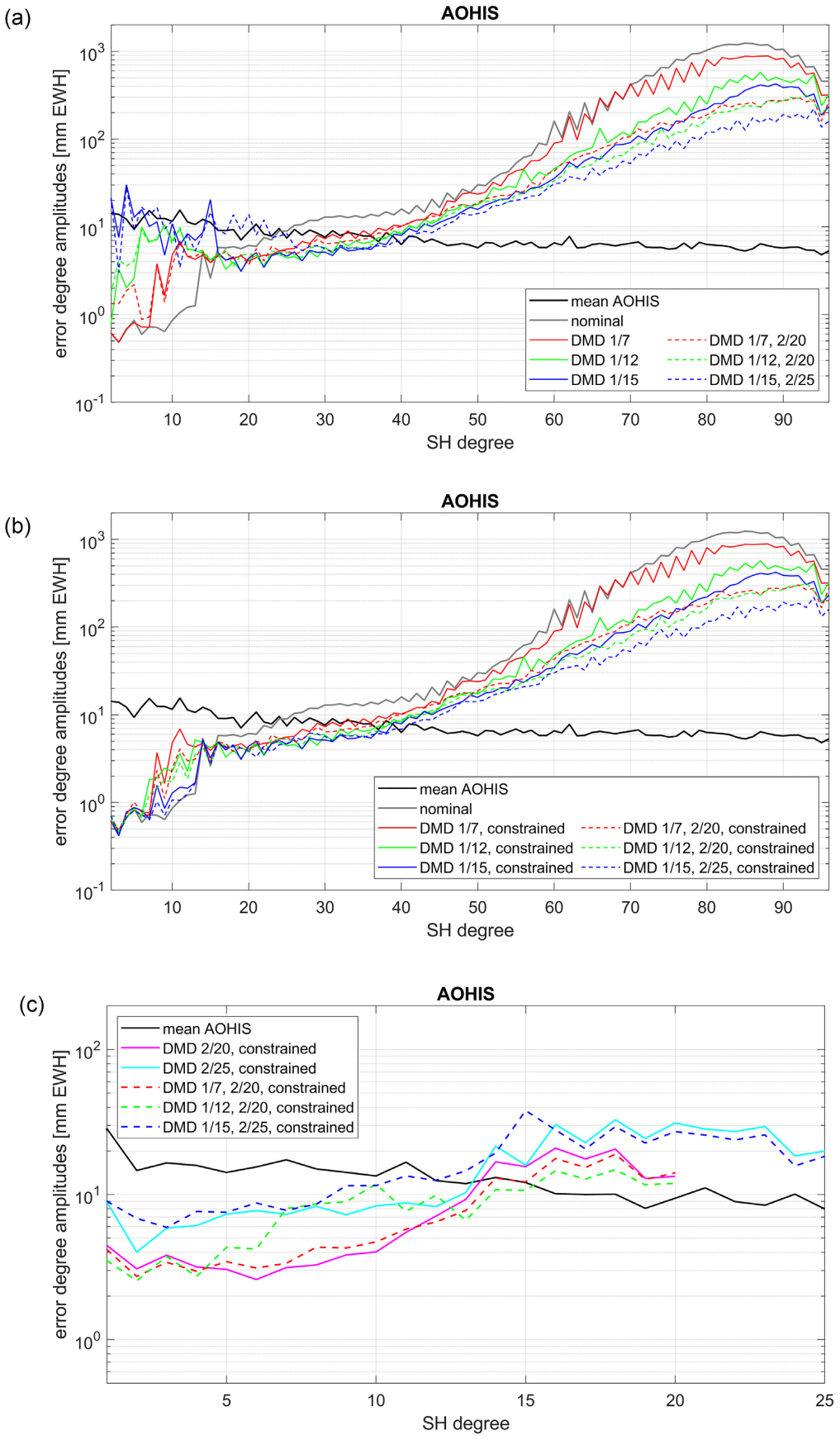

Figure 7. Retrieval error of the 1-pair-based 30-d solutions based on the full AOHIS signal under employment of various unconstrained (a) and constrained (b) single- and multi-period DMD schemes. (c) Mean retrieval error of the 2-d fields of various DMD schemes.

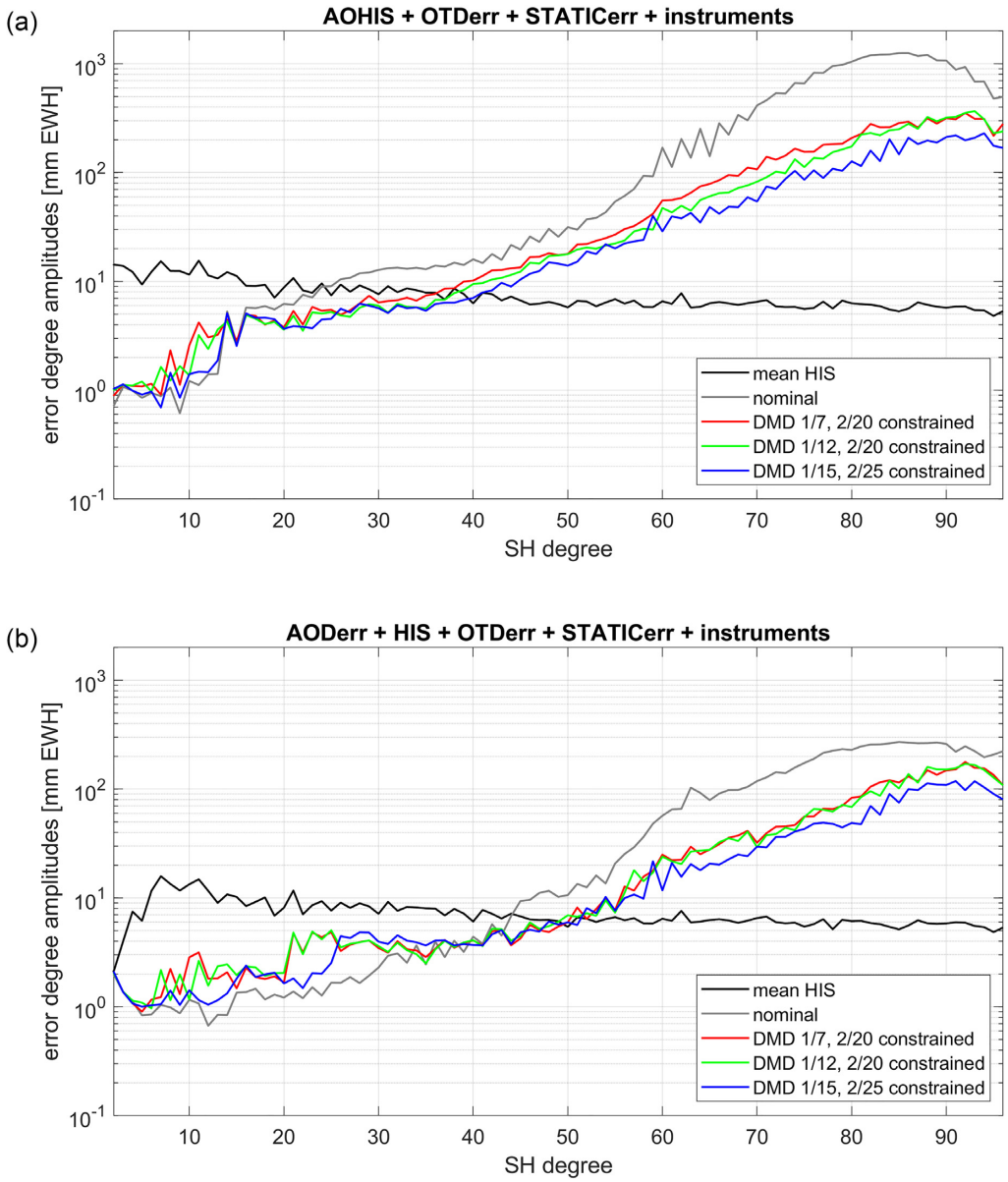

Figure 8. Retrieval error of the 1-pair-based 30-d solution under employment of various constrained and unconstrained multi-period DMD schemes. In a) the full AOHIS as well as the residual OT signal and the instrument noise is considered while in b) the AO component's amplitudes are reduced to 10 per cent of their original value in order to simulate BM-based AO de-aliasing.

static field's error can be considered as negligible throughout the most part of the spectrum and only contributes to a minor extent to the total retrieval error from d/o 70 upwards.

The corresponding results are depicted in Fig. 8(b). It can be asserted that, similarly to the full-AOHIS case, the DMD significantly improves the retrieval within the high-degree spectrum. In this way, a maximum retrieval error reduction of up to 70 per cent in case of the constrained DMD 1/7, 2/20 and DMD 1/12, 2/20 as well as up to 80 per cent in case of the constrained DMD 1/15, 2/25 with respect to the nominal processing can be established in the spectral range above d/o 65. All three DMD scenarios also allow for a reliable HIS retrieval up to around d/o 52, while the nominal processing only allows to retrieve the HIS signal up to *ca.* d/o 45. On the other hand, even though the constraint is applied in the shown DMD scenarios, the DMD-based retrieval nevertheless features some level of degradation in the spectral range between d/o 5 and 30. However, even though these deteriorations are quite notable (up to 70 per cent compared to the nominal case), the SNR still remains well below 1 in the affected spectral bands.

4.3. Outlook to application in double-pair scenarios

In a final set of simulations, we give a brief outlook towards the DMD's functionality in the context of Bender-type double-pair-based gravity retrieval (*cf.* Table 1). Here, we once again consider the full noise scenario and attempt to retrieve both the full AOHIS signal as well as

only the HIS component by applying model-based de-aliasing for AO over a total period of 30 days. DMD 1/15 as a single-period scheme in addition to DMD 1/20, 2/40 and DMD 1/15, 2/30, 3/45 as multi-period schemes as well as their respective constrained equivalents are applied. The time intervals and spatial resolutions of the first and last DMD schemes are chosen in such a way that the Nyquist-Colombo theorem can be considered as fulfilled. DMD 1/20, 2/40 is chosen because pushing past the theoretical resolvable maximum degree has been proven beneficial for the overall performance of the monthly product in the single-pair case. In addition, the DMD's performance is compared against that of the standard two-step co-parametrization with daily fields up to d/o 15.

The results concerning the retrieval of the full AOHIS signal are presented in Fig. 9(a). First, it can be seen that some improvements with respect to the nominal processing approach can be achieved with the standard 2-step 1/15 scheme. These manifest primarily in the spectral bands between d/o 13 and 25 as well as upwards from d/o 50 where they constitute up to 40 per cent and 20 per cent, respectively. It can further be established that while all unconstrained DMD schemes show partial improvements over the nominal approach below d/o 45, the multi-period schemes also lead to some level of degradation. These deteriorations are, however, significantly less severe than in the single-pair case and can be regarded as negligible, as the SNR is still well below 1. Nevertheless, they can still be reduced by applying the additional constraint towards the nominal solution as discussed earlier. The DMD's main value once again primarily manifests within the higher degrees of the monthly solution. Above d/o 50, the retrieval performance can be improved by more than 25 per cent in case of DMD 1/15 and by more than 50 per cent in case of DMD 1/20, 2/40 and DMD 1/15, 2/30, 3/45 (both constrained and unconstrained). In this way, the full AOHIS signal can be retrieved reliably up to *ca.* d/o 59 with DMD 1/15, 2/30, 3/45, in case of the nominal processing the threshold lies at *ca.* d/o 53.

As can be seen in Fig. 9(b), the overall value of the DMD approach decreases slightly once BM-based de-aliasing is applied for the AO component. Here, even the constrained DMD schemes result in some level of deterioration in the spectral range below d/o 50. Above d/o 50, DMD 1/15 yields up to 15 per cent improvement over the nominal solution, while DMD 1/15, 2/30, 3/45 reduces the retrieval error by up to 40 per cent. The HIS signal can be retrieved up to *ca.* d/o 60 by means of the nominal processing, while DMD 1/15, 2/30, 3/45 allows for its retrieval up to d/o 63. However, it is quite notable that the two-step co-parametrization yields a near-identical solution as the nominal processing, i.e. contrary to the previously discussed full AOHIS case, no notable improvements can be established with this method in this scenario.

With regard to the quality of the monthly solution, it can be concluded that the DMD approach (even when considering the slight degradations in the respective solutions' lower-degree spectrum) is overall superior to the two-step co-parametrization. With regard to the (co-)estimated interval fields, however, the situation is slightly different. As can be seen in Fig. 9(c), in case of the full AOHIS signal the 2-step-based daily d/o 15 fields seem to feature an up to 15 per cent lower average error above d/o 10. Although not quite comparable, a similar tendency can be found in case of the daily fields obtained with DMD 1/20. In the scenario where the AO component is reduced *a priori*, the variations become even larger and thus, the 2-step-based d/o 15 fields outperform the DMD-based ones by up to 30 per cent. Overall, however, both the DMD and the two-step co-parametrization yield reliable daily estimates (once again, SNR < 1).

In total, the DMD can be regarded as at least equivalent to the standard two-step co-parametrization approach if applied in the context of a Bender-type constellation. Due to the evidently enhanced performance of the 2-step-based interval fields, it might be of interest to employ them within the DMD procedure and to investigate the resulting impact. Also, further studies shall be carried out in order to determine the optimal DMD parameters within the scope of double-pair-based processing.

5 DMD PERFORMANCE VALIDATION IN REAL DATA PROCESSING

In this section, we describe the methodology and results regarding the performance of the DMD in real GRACE and GRACE-FO data processing. Here, we compare monthly gravity fields retrieved on the basis of the GFZ GRACE RL06 processing scheme (Dahle *et al.* 2019) to fields obtained based on the same scheme extended with the unconstrained single-period DMD. The GFZ GRACE/GRACE-FO monthly gravity field solutions are based on daily combined GPS and K-Band range-rate (KRR) NEQ systems which are accumulated over the period of one month. The DMD uses these daily NEQs in a first step in order to estimate the daily low-resolution fields. As already noted in Section 3, in this first step it is imperative to deal with the high-degree static gravity signal in order to minimize spectral leakage. In the real data case, this issue is treated by fixing the high-degree signal (above the maximum degree of expansion of the daily solutions) to an *a priori* static gravity model. After the daily fields are estimated, the observation vector is reduced only by their variations to their monthly mean, i.e. no restoration step as denoted in Eq. (15) is required. It is noted that real data tests are performed only for a scenario where all de-aliasing models within GFZ GRACE/GRACE-FO RL06 Level 2 processing are used (AOD, Dobslaw *et al.* 2017 and the OT model FES2014, Lyard *et al.* 2021). All other processing steps remain identical to the standard GFZ RL06 Level 2 processing strategy.

Further, it is noted that in comparison to the simulation environment with perfect conditions the issue of inhomogeneous data coverage must be handled here. Each of the processed months features between zero and five daily estimates of low quality, which can for the most part be attributed to missing or flagged data (e.g. due to instrument malfunctions, recalibrations, orbital manoeuvres) in combination with bad global coverage. Therefore, such daily solutions are treated as outliers which are excluded from the second step. Instead, we replace the omitted daily solutions for these specific intervals by interpolated ones based on the neighbouring 'good' solutions applying linear interpolation.

The first investigation is related to the question regarding what type of daily solution is best suited for the DMD scheme. The tests are performed up to max. d/o 96. Besides the daily solutions validated in the simulated cases, i.e. estimates up to max. d/o 7, 12 and 15 based exclusively on the observations of a single day (in the following denoted as DS07, DS12, DS15), we also use daily solutions up to max. d/o

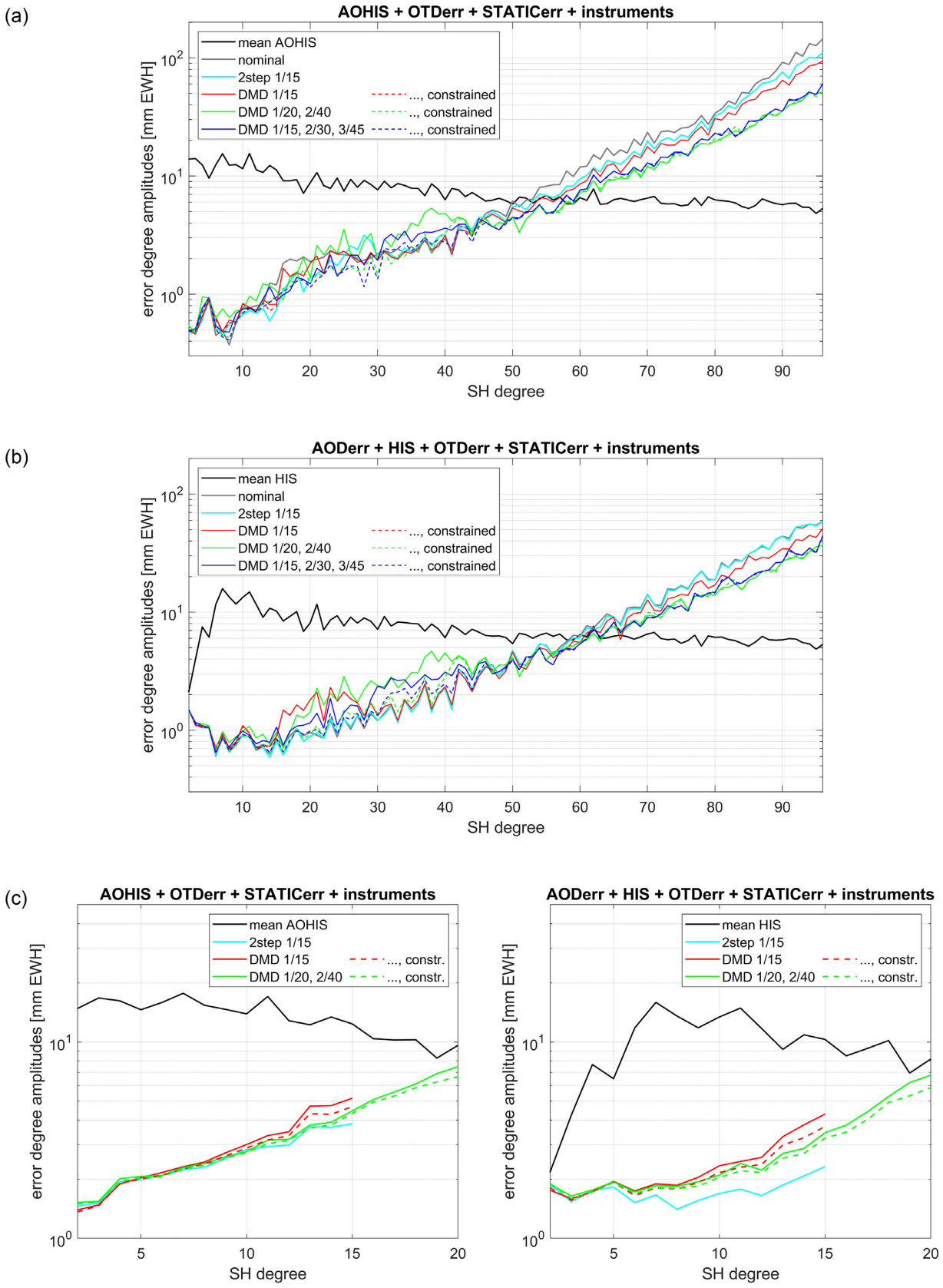

Figure 9. Retrieval error of the 2-pair-based 30-d solution under employment of various constrained and unconstrained multi-period DMD schemes as well as the standard two-step co-parametrization. In (a), the full AOHIS as well as the residual OT signal and the instrument noise is considered while in (b), the AO component's amplitudes is reduced to 10 per cent of their original value in order to simulate BM-based AO de-aliasing. Panel (c) shows the retrieval error of DMD- and two-step-co-parametrization-based daily fields for the scenarios presented in (a) and (b).

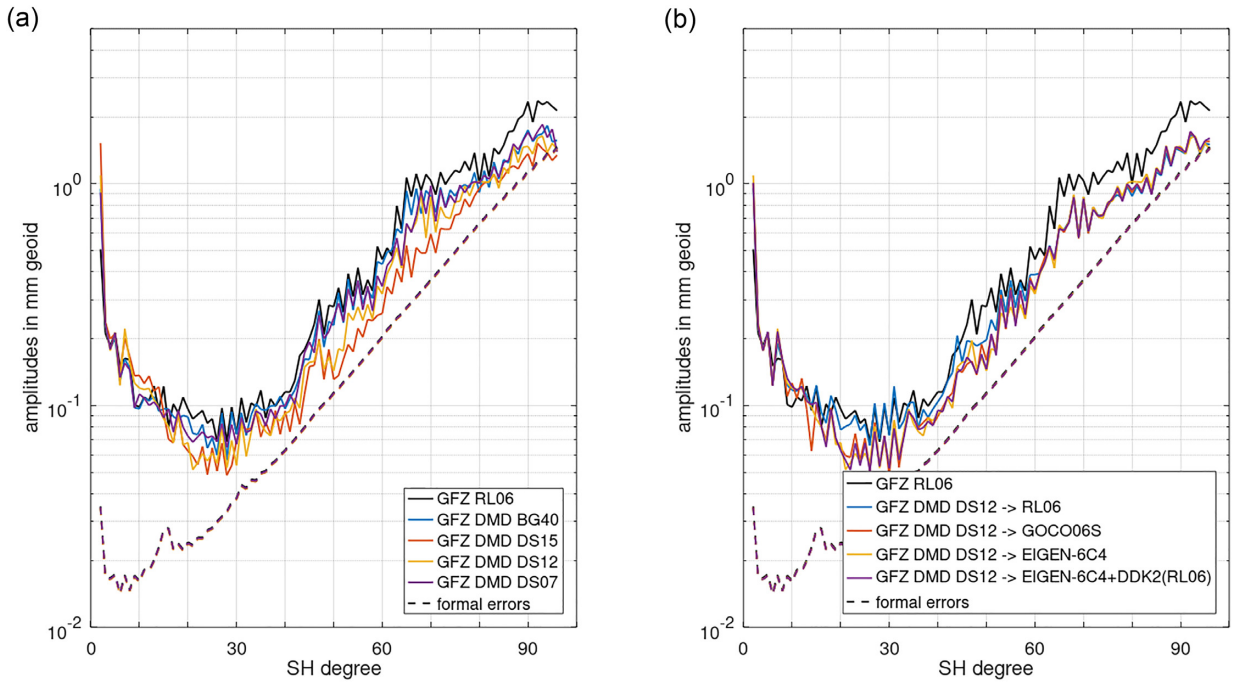

Figure 10. Spherical harmonic degree amplitudes in mm geoid heights for different DMD residuals w.r.t. a GFZ GRACE RL06 climatology for November 2007 and corresponding formal errors, compared to and based on the GFZ GRACE RL06 processing (black). (a) Comparison of different daily solutions, that is a Gaussian weighted 15 d moving window solution up to degree and order (d/o) 40 (BG40), and daily solutions using only the observations of one day up to different max. d/o 15, 12, and 7 (DS15, DS12, DS07). (b) DMD solutions with DS12 using different *a priori* fields for fixing the spherical harmonic coefficients above degree 12, that is the standard monthly GFZ RL06 solution (blue), GOCO06S (evaluated for the mean epoch of that month, red), EIGEN-6C4 (yellow), and EIGEN-6C4 plus the DDK2 filtered monthly GFZ RL06 solution (purple).

40 where we accumulate 15 daily NEQs weighted with a Gaussian weighting scheme (BG40). Hence, the latter have higher spatial, but lower temporal resolution in comparison to the DS scenarios. The residuals of the different monthly solutions with respect to (w.r.t.) a GRACE climatology (6 parameter model estimated in terms of spherical harmonic coefficients from the whole GFZ GRACE RL06 time series) in terms of degree amplitudes are shown in Fig. 10(a). Here, a significant noise reduction for all four investigated DMD cases can be seen in the spectral bands above d/o 30 which is strongest for DS12 and DS15. At the same time, however, some level of degradation in the low degrees can also be noted for these two scenarios. Since the constraint is not applied here, these results are in full accordance with the findings obtained in the simulated scenarios. Because the error is substantial in case of DS15, the DS12 scenario is used for all following tests.

In the second set of tests we aim to clarify the impact of the chosen *a priori* static gravity field model to whose values the spherical harmonic coefficients of high degrees are fixed on the overall DMD performance. Here, we use EIGEN-6C4 (Förste *et al.* 2014, applied in the first set of tests), the standard GFZ RL06 solution of the respective month, the static field GOCO06s (evaluated for the mean epoch of the respective month) and, finally, EIGEN-6C4 complemented by a DDK2-filtered (Kusche *et al.* 2009) monthly GFZ RL06 solution. The results are presented in Fig. 10(b). While above d/o 60 a comparable noise reduction can be established for all four scenarios, for the medium and lower spherical harmonic degrees the version using the unfiltered GFZ RL06 monthly field seems to perform the worst. On the other hand, the different static field variants show a better performance and the differences between these three scenarios can be described as minor. It can thus be concluded for the fixing of the daily solutions' high degrees the application of a static field which is not affected by typical GRACE-like error patterns (striping) is preferable. Additionally, the consideration of (approximate) time-variable signal content such as in case of GOCO06s and the EIGEN-6C4 augmented with the filtered GFZ RL06 solution is of minor importance.

Further, we validate the performance of the DMD over time spans of one year. Here, we process all monthly solutions of 2007, 2014 (GRACE) and 2019 (GRACE-FO) based on DS12 with the interval solutions' high degrees fixed to EIGEN-6C4 and compare the results to the standard GFZ RL06 solutions (*cf.* Fig. 11). It is evident that the DS12 approach yields a significant noise reduction of up to 30 per cent, especially in the high degrees. However, major performance differences can be seen between the three test years. While in 2007 and 2014 the residuals are reduced for nearly all spherical harmonic degrees, in 2019, which is a GRACE-FO year, this is the case only for d/o 70 and higher. Regarding the low-degree spectrum, all test years feature increased residuals around d/o 10 in comparison to the standard GFZ RL06. This behaviour is most likely attributed to the previously discussed shortcomings of the unconstrained DMD scheme. On the right-hand side of Fig. 11, the spatial relative residual change for 300 km Gaussian-filtered solutions is shown. For 2007, and to a lesser extent also for 2014, the residual RMS (assumed to be dominated by noise) reduction is seen globally with maximum values in oceanic regions. As could already be deduced from the spectral comparisons, no noise reduction of similar extent can be seen for 2019.

Originally, the DMD performance differences between the GRACE and GRACE-FO years were speculated to be related to certain intrinsic problems of the GRACE-FO mission (e.g. the missing accelerometer observations on one of the satellites) or to a varying quality

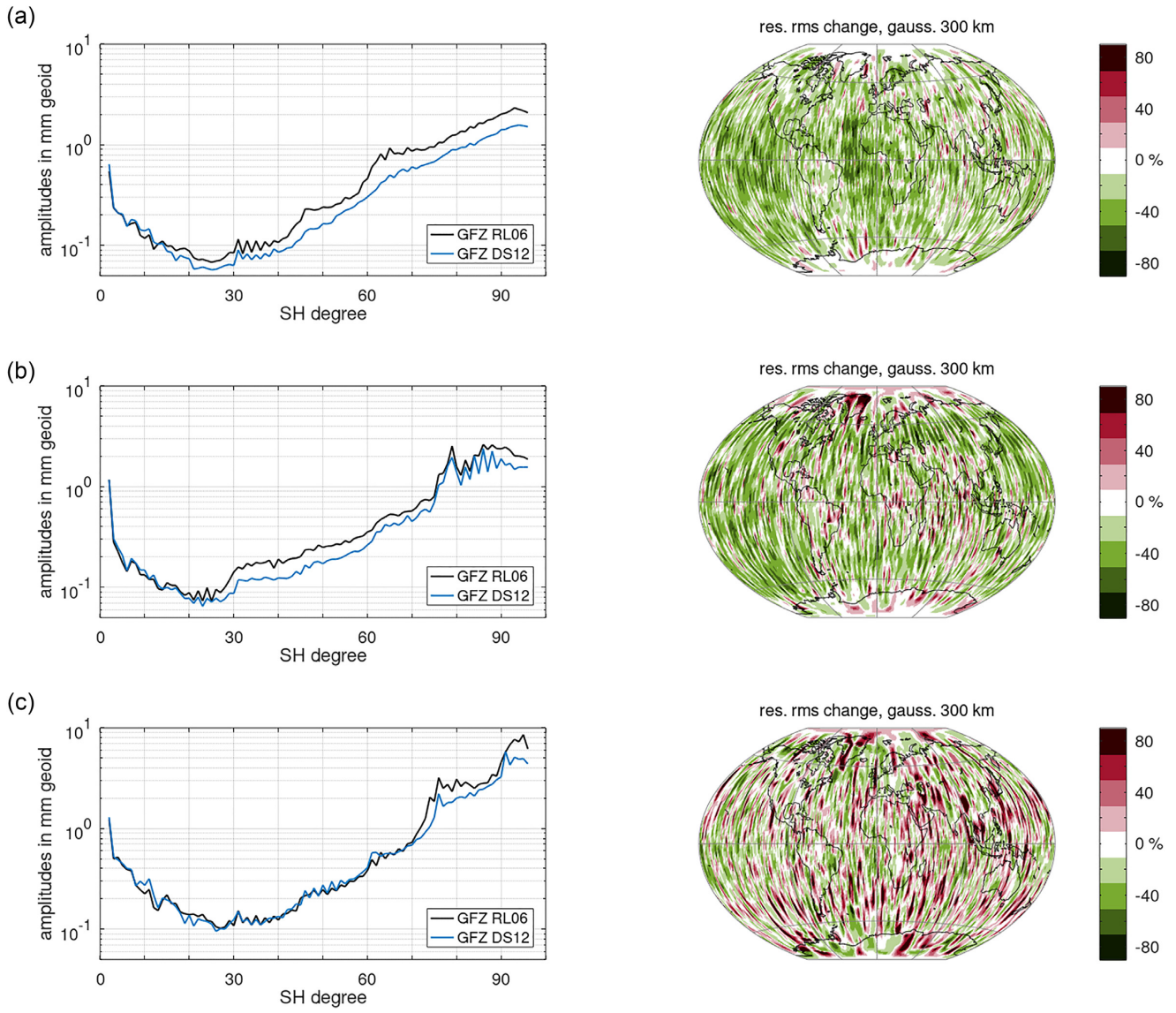

Figure 11. Comparison of DMD residuals w.r.t. a GFZ GRACE RL06 climatology using DS12 with fixing high degrees to EIGEN-6C4 for the years 2007 (a), 2014 (b) and 2019 (c) compared to GFZ GRACE/GRACE-FO RL06. Left: Spherical harmonic degree amplitudes of the residual RMS of all monthly solutions of that year in mm geoid height. Right: relative spatial residual RMS change of 300 km Gaussian filtered solutions when applying the DMD to GFZ GRACE/GRACE-FO RL06 in per cent.

of de-aliasing models applied for these periods. The likeliest reason, however, is found in the fact that the separation of the parameter space carried out in the frame of the DMD scheme results in a bias towards the applied background models. In other words, the produced solutions encompass a weighted mean of the background models and the true observations. This issue is discussed in detail in Meyer *et al*. (2015). There, it is also shown that the 'weight' of the BMs is essentially inversely proportional to their quality, as any mismodelled or neglected gravity signals there will be attenuated in the final product. In the case at hand, the critical issue is the EIGEN-6C4 model used to treat the high-degree static gravity signal. Note that EIGEN-6C4 is comprised of GRACE data from the period between 2003 and 2012 in the relevant spectral range, so its reference epoch lies somewhere around the years 2007–2008. This explains the very good performance of the DMD scheme for the year 2007, but since the same model is used also for the other test years without considering the static signal's temporal evolution, a larger bias is induced in the 2014 solutions and especially in the 2019 ones, thus degrading the overall performance. The impact of the static background model is essentially also evident in Fig. 10(b), where a significant deterioration with RL06 which especially in the high degrees contains a significant amount of noise can be seen in comparison to EIGEN-6C4 and GOCO06s (whose reference epoch is 2010). The impact of the bias is further demonstrated in Fig. 12 which shows the results of a DMD-based solution for January 2019 with and without adjusting the reference epoch of EIGEN-6C4. This was achieved by modulating its signal with the trends given in GOCO06s. Here, the solution using the reference-adjusted static field improves by up to 30 per cent in the medium- to high-degree range in comparison to the case where its reference epoch remains in 2007. Also, notable improvements of up to 15 per cent can be seen in the lower degrees. Using a

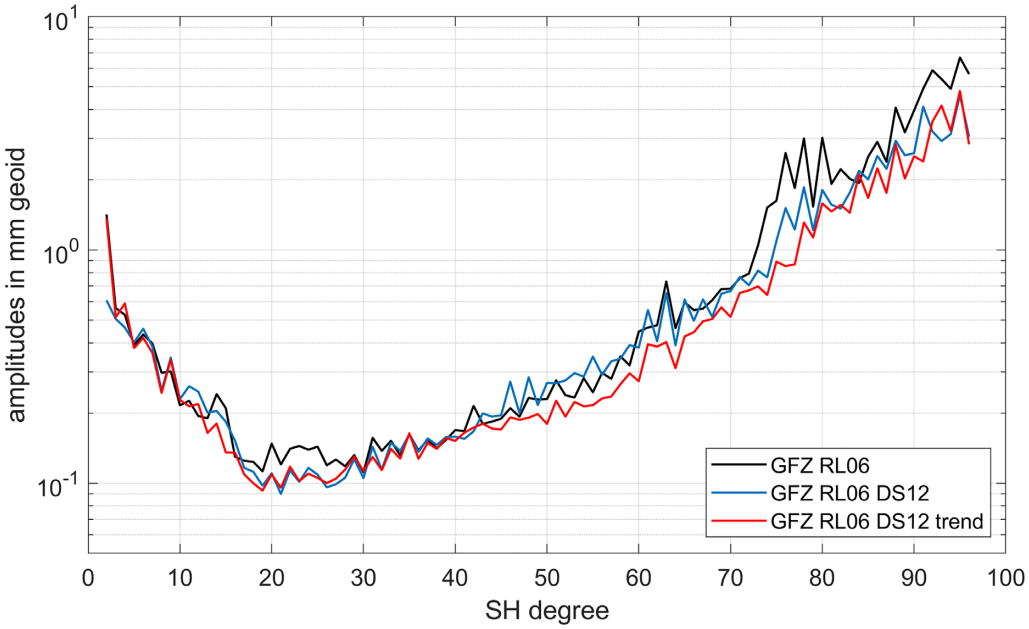

Figure 12. Spherical harmonic degree amplitudes for January 2019 w.r.t. a GFZ GRACE RL06 climatology based on the standard RL06 processing scheme, RL06 including DMD 1/12 with EIGEN-6C4 as static reference and RL06 including DMD 1/12 with EIGEN-6C4 an adjusted reference epoch through consideration of the trend signal from GOCO06s.

static field of the highest-possible quality is thus crucial to minimize the solution bias and thus maximize the added value of the DMD. The presented results show that the remaining bias can be accepted, as for the most part it is outweighed by the noise reduction.

Overall, it can be stated that the real data results fully support the findings obtained within the simulation studies in term of noise reduction for medium to high degrees (*cf.* Figs 11 and 8b). Because the constraint has not yet been applied within the real data processing, it can be expected that the occurring errors within certain low-degree bands can also ultimately be reduced.

6 CONCLUSIONS AND OUTLOOK

In this paper we present and discuss a data-driven multi-step self-de-aliasing approach (DMD) for single-pair-based gravity retrieval, and investigate its impact within numerical closed-loop simulations and within real data processing. Within the DMD, low-resolution gravity fields are estimated over short time intervals, the corresponding signals are reduced from the satellites' observation time series and the reduced observations are in turn used to estimate a long-term, e.g. monthly gravity solution to which the interval fields' mean is restored in a final step. In this way, the short-periodic long-wavelength signals which are predominantly related to the time-variable AO component can be captured within the interval fields and thus prevented from manifesting as temporal aliasing effects, i.e. striping, within the long-term solution. Simultaneously, the interval solutions pose stand-alone gravity products for the respective time frames. It is shown that this separation of the parameter space is necessary to circumvent the shortcomings of the standard two-step co-parametrization presented in Wiese *et al.* (2011). While the DMD inevitably induces certain misparametrization errors, these are widely outweighed by its aliasing reduction capabilities, and an enhanced retrieval of the full AOHIS signal is facilitated without the requirement of application of geophysical background models.

The DMD's overall performance depends on the chosen spatial resolution of the interval fields. It can be shown that a higher resolution significantly improves the monthly estimate's high-degree spectrum due to the reduced aliasing, but, simultaneously, the low degrees are degraded due to leakage effects. For the most part, this issue can be successfully remedied by constraining the interval fields' mean to the corresponding part of the nominal solution, i.e. one obtained without any additional parametrization. This constraint is also purely data-driven. The added value of the constraint can also be clearly seen within the interval fields themselves—these can be improved by up to 70 per cent in certain spectral bands.

It is further shown that the DMD scheme is not limited to the estimation of interval fields for just a single time period, but can in principle be extended by a number of intermediate steps before estimating the final monthly gravity product. Analogously to the regular, i.e. single-period, DMD, also here the constraint can be applied. It is demonstrated that the interval estimates obtained from subsequent iterations already show a somewhat decreased performance due to misparametrization errors. Within the monthly estimate, however, the effect of aliasing reduction still dominates and its retrieval performance can be further increased by 40 to 70 per cent in comparison to the results obtained with single-period DMD schemes.

In total, the DMD-based retrieval of the full monthly AOHIS signal can be enhanced by up to one order of magnitude with respect to the nominal processing scheme. In this way, a reliable retrieval is shown to be possible up to d/o 40, while in case of the nominal processing the maximum degree of resolution lies at around 25. Furthermore, the DMD also shows significant value even when applied in combination

with *a priori* AO de-aliasing based on geophysical background models. Since the DMD is also capable of reducing OT- and HIS-induced aliasing effects in the short-wavelengths spectrum, the maximum retrievable degree of the HIS signal is increased here from around 45 to 50 in comparison to the nominal gravity retrieval.

The DMD is also shown to be applicable and overall beneficial for the double-pair-based gravity retrieval. In this way, the full AOHIS signal can be retrieved up to d/o 60 over the course of one month as opposed to d/o 53 with the nominal processing. In the case of *a priori* de-aliasing of AO components, the retrieval performance of the HIS signal can be increased by up to 40 per cent in the high-degree spectrum, although the maximum resolvable degree does not change notably. Furthermore, it is established that the DMD scheme outperforms the standard two-step co-parametrization in both scenarios. However, it is also shown that the interval estimates obtained with the two-step co-parametrization approach show a better performance than those obtained with DMD (up to *ca.* 15 per cent in case of full-AOHIS retrieval and up to *ca.* 30 per cent when *a priori* de-aliasing is done for AO).

The findings obtained in the simulation environment are substantiated through the real data results obtained from the application of DMD to the processing chain. Here, the unconstrained single-period DMD is applied to the standard processing scheme of GFZ GRACE/GRACE-FO RL06 with interval solutions of various spatial and temporal resolution. The analyses of monthly solutions for two GRACE- and one GRACE-FO-based test years show a significant noise reduction of up to 30 per cent for medium and spherical harmonic degrees. However, also a possible error increase in the very low degrees can be established, although this behaviour can likely be rectified by introducing the constraint. The real data results also clearly demonstrate that a static background model of the highest-possible quality is required in order to minimize the bias onto the final product and thus fully exploit the noise reduction potential of the DMD.

In summary, the value of the DMD for GRACE/GRACE-FO-type data processing is clearly demonstrated. In future research, improved methods for the treatment of high-degree signal components shall be investigated in order to further reduce leakage errors. Further studies concerning the multi-period DMD shall be conducted in order to find the most optimal parameter model both for the interval fields as well as for the long-term estimate. Future work in regard to real data shall focus on the implementation of the constraint for the low degrees when estimating the interval solutions. Also, longer time series shall be investigated in order to help understand the DMD's potential dependencies on and interactions with the underlying ground track coverage. Especially its performance in so-called 'bad months' featuring deep-resonance repeat cycles of a few days, will be of great interest here. With regard to the DMD in the frame of double-pair-based gravity retrieval, it may prove valuable to employ the interval fields obtained with the two-step co-parametrization approach within the DMD's observation reduction step, as these have been shown to be of an overall better quality than the ones retrieved with the DMD.

ACKNOWLEDGMENTS

The work presented in this paper was performed within the framework of the project 'New Refined Observations of Climate Change from Spaceborne Gravity Missions (NEROGRAV)' funded by the German Research Foundation (Research Unit FOR 2736/1). We also acknowledge the provision of supercomputing resources by the Leibniz Supercomputing Centre (LRZ, Address: Boltzmannstraße 1, 85748 Garching bei München, Germany).

DATA AVAILABILITY

The data that support the findings of this study are openly available upon reasonable request to the corresponding author.

REFERENCES

Abelen, S., Seitz, F., Abarca-del-Rio, R. & Güntner, A. 2015. Droughts and floods in the La Plata Basin in soil moisture data and GRACE, *Remote Sens.,* **7,** 7324–7349.

Abrykosov, P., Sulzbach, R., Pail, R., Dobslaw, H. & Thomas, M. 2021. Treatment of ocean tide background model errors in the context of GRACE/GRACE-FO data processing, *Geophys. J. Int.,* **228,** 1850–1865.

Bender, P. L., Wiese, D. N. & Nerem, R. S. 2008. A possible dual-GRACE mission with 90 degree and 63 degree inclination orbits, in *Proceedings, 3rd International Symposium on Formation Flying. Missions and Technologies,* ESA/ESTEC, Noordwijk, pp. 1–6.

Colombo, O. 1984. The global mapping of gravity with two satellites, In: *Netherlands Geodetic Commission, in publications on Geodesy,* vol **7**(3).

Dahle, C. *et al.* 2019. The GFZ GRACE RL06 monthly gravity field time seires: processing details and quality assessment, *Remote Sens.,* **11**(18), 2116.

Daras, I. 2016. Gravity field processing towards future LL-SST satellite missions. Deutsche Geodätische Kommission der Bayerischen Akademie der Wissenschaften, Reihe C, Dissertationen, Heft 770, *Verlag der Bayerischen Akademie der Wissenschaften,* ISBN(Print) 978-3-7696-5182-9, ISSN 0065-5325, 2016.

Daras, I. & Pail, R. 2017. Treatment of temporal aliasing effects in the context of next generation satellite gravimetry missions, *J. geophys. Res.,* **122**(9), 7343–7362.

Dobslaw, H. *et al.* 2013. Simulating high-frequency atmosphere-ocean mass variability for de-aliasing of satellite gravity observations: AOD1B RL05, *J. geophys. Res.,* **118**(7), 3704–3711.

Dobslaw, H. *et al.* 2017. A new high-resolution model of non-tidal atmosphere and ocean mass variability for de-aliasing of satellite gravity observations: AOD1B RL06, *Geophys. J. Int.,* **211,** 263–269.

Dobslaw, H., Bergmann-Wolf, I., Dill, R., Forootan, E., Klemann, V., Kusche, J. & Sasgen, I. 2014. The updated ESA earth system model for gravity mission simulation studies, *J. Geod.,* **89**(5), 505–513.

Flechtner, F., Neumayer, K. H., Dahler, C., Dobslaw, H., Fagiolini, E., Raimondo, J. C. & Güntner, A. 2016. What can be expected from the GRACE-FO laser ranging interferometer for earth science applications?, *Surv. Geophys.,* **37**(2), 453–470.

Flechtner, F., Reigber, C., Rummel, R. & Balmino, G. 2021. Satellite gravimetry: a review of its realization, *Surv. Geophys.,* **42**(5), 1029–1074.

Förste, C. *et al.* 2014. *EIGEN-6C4 The Latest Combined Global Gravity Field Model Including GOCE Data up to Degree and Order 2190 of GFZ Potsdam and GRGS Toulouse,* GFZ Data Services.

Han, S., Ray, R. & Luthcke, S., 2007. Ocean tidal solutions in Antarctica from GRACE inter-satellite tracking data, *Geophys. Res. Lett.,* **34,** L21607, doi:10.1029/2007GL031540.

Hauk, M. & Pail, R., 2018. Treatment of ocean tide aliasing in the context of a next generation gravity field mission, *Geophys. J. Int.,* **214**(1), 345–365.

Iran Pour, S. *et al.* 2015. Assessment of Satellite Constellations for Monitoring the Variations in Earth Gravity Field "SC4MGV", ESA – ESTEC Contract No. AO/1-7317/12/NL/AF, Final Report.

Killett, B., Wahr, J., Desai, S., Yuan, D. & Watkins, M., 2011. Arctic Ocean tides from GRACE satellite accelerations, *J. geophys. Res.,* **116,** C11005.

Kornfeld, R. P., Arnold, B. W., Gross, M. A., Dahya, N. T., Klipstein, W. M., Gath, P. F. & Bettadpur, S., 2019. GRACE-FO: the gravity recovery and climate experiment follow-on mission, *J. Spacecr. Rockets,* **56**(3), 931–951.

Kusche, J., Schmidt, R., Petrovic, S. & Rietbroek, R. 2009. Decorrelated GRACE time-variable gravity solutions by GFZ, and their validation using a hydrological model, *J. Geod.,* **83,** 903–913.

Kvas, A. *et al.* 2019. The satellite-only gravity field model GOCO06s, GFZ Data Services. http://doi.org/10.5880/ICGEM.2019.002

Kvas, A. *et al.* 2021. GOCO06s—a satellite-only global gravity field model, *Earth Syst. Science Data,* **13**(1), 99–118.

Kvas, A. & Mayer-Gürr, T. 2019. GRACE gravity field recovery with background model uncertainties, *J. Geod.,* **93,** 2543–2552.

Lyard, F. H., Allain, D. J., Cancer, M., Carrère, L. & Picot, N. 2021. FES2014 global ocean tide atlas: design and performance, *Ocean Sci.,* **17,** 615–649.

Mayer-Gürr, T., Savcenko, R., Bosch, W., Daras, I., Flechtner, F. & Dahle, C., 2012. Ocean tides from satellite altimetry and GRACE, *J. Geodyn.,* **59-60,** 28–38.

Meyer, U., Jäggi, A., Beutler, G. & Bock, H. 2015. The impact of common versus separate estimation of orbit parameters on GRACE gravity field solutions, *J. Geod.,* **89**(7), 685–696.

Mulder, G., Olsthoorn, T. N., Al-Manmi, D., Schrama, E. J. O. & Smidt, E. H. 2015. Identifying water mass depletion in northern Iraq observed by GRACE, *Hydrol. Earth Syst. Sci.,* **19,** 1487–1500.

Murböck, M. 2015. Virtual constellations of next generation gravity missions. Deutsche Geodätische Komission der Bayerischen Akademie der Wissenschaften, Reihe C, Dissertationen, Heft 750, *Verlag der Bayerischen Akademie der Wissenschaften,* ISBN(Print) 978-3-7696-5162-1, ISSN 0065-5325, 2016.

Murböck, M., Pail, R., Daras, I. & Gruber, T. 2014. Optimal orbits for temporal gravity recovery regarding temporal aliasing, *J. Geod.,* **88**(2), 113–126.

Pail, R. *et al.* 2018. Additional Constellation & Scientific Analysis of the Next Generation Gravity Mission Concept "ADDCON" – ESA Contract No. 4000118480/16/NL/FFgp, Final Report.

Purkhauser, A. F. & Pail, R. 2019. Next generation gravity missions: near-real time gravity field retrieval strategy, *Geophys. J. Int.,* **217**(2), 1314–1333.

Purkhauser, A. F., Siemes, C. & Pail, R. 2020. Consistent quantification of the impact of key mission design parameters on the performance of next-generation gravity missions, *Geophys. J. Int.,* **221**(2), 1190–1210.

Ray, R. 1999. *A global ocean tide model from TOPEX/POSEIDON altimetry*. GOT99.2. Rep NASA/TM-1999-209478, 58pp., Goddard Süace Flight Center, Greenbelt, Maryland.

Reager, J. T., Thomas, B. F. & Famiglietti, J. S. 2014. River basin flood potential inferred using GRACE gravity observations at several months lead time, *Nat. Geosci.,* **7,** 588–592.

Rudenko, S., Dettmering, D., Esselborn, S., Fagioloni, E. & Schöne, T. 2016. Impact of atmospheric and oceanic de-aliasing level-1B (AOD1B) products on precise orbits of altimetry satellites and altimetry results, *Geophys. J. Int.,* **204,** 1695–1702.

Savchenko, R. & Bosch, W. 2012. *EOT11a—Global Empirical Ocean Tide model from multi-mission satellite altimetry,* DGFI Report No. 89, München: Deutsches Geodätisches Forschungsinstitut

Shannon, C. E. 1949. Communications in the presence of noise, *IEEE Proc.,* **37,** 10–21.

Shepherd, A., Ivins, E. R., Geruo, A., Barletta, V. R., Bentley, M. J., Bettadpur, S. & Zwally, H. J. 2012. A reconciled estimate of ice-sheet mass balance, *Science,* **338**(6111), 1183–1189.

Shihora, L., Balidakis, K., Dill, R., Dahle, C., Ghobadi-Far, K., Bonin, J. & Dobslaw, H. 2022. Non-tidal background modelling for satellite gravimetry based on operational ECWMF and ERA5 reanalysis data AOD1B RL07, *J. geophys. Res.,* **127**(8). doi: 10.1029/2022JB024360.

Tapley, B., Bettadpur, S., Watkins, M. & Reigber, C., 2004. The gravity recovery and climate experiment: mission overview and early results, *Geophys. Res. Lett.,* **31**(9), L09607, doi: 10.1029/2004GL019779.

Velicogna, I., Scutterley, T. C. & van den Broeke, M. R. 2014. Regional acceleration in ice mass loss from Greenland and Antarctica using GRACE time-variable gravity data, *Geophys. Res. Lett.,* **41**(22), 8130–8137.

Weigelt, M., Sneeuw, N., Schrama, E. J. O. & Visser, P. 2013. AN improved sampling rule for mapping geopotential functions of a planet from a near polar orbit, *J. Geod.,* **87,** 127–142.

Wiese, D. N., Visser, P. & Nerem, R. S. 2011. Estimating low resolution gravity fields at short time intervals to reduce temporal aliasing errors, *Adv. Space Res.,* **48**(6), 1094–1107.

Yang, F., Forootan, E., Wang, C. Q., Kusche, J. & Luo, Z. C. 2021. A new 1-hourly ERA5-based atmosphere de-aliasing product for GRACE, GRACE-FO, and future gravity missions, *J. geophys. Res.,* **126**(9), e21926, doi:10.1029/2021JB021926.